JEM Journal of Experimental Medicine

ARTICLE

Invariant TCR-triggered protein kinase D activation mediates NKT cell development

Eri Ishikawa[1,2], Hidetaka Kosako[3], Daisuke Motooka[4], Mai Imasaka[5], Hiroshi Watarai[6], Masaki Ohmuraya[5], and Sho Yamasaki[1,2,7,8]

Development of invariant natural killer T (iNKT) cells in the thymus requires cell–cell interaction through invariant TCR (iTCR) and CD1d, which induces expression of the transcription factor, promyelocytic leukemia zinc finger (PLZF). However, the signaling pathway linking iTCR and PLZF remains unclear. Here, we report that a serine/threonine kinase, protein kinase D (PKD), plays a pivotal role in iNKT cell development. In T cell–specific PKD-deficient (*Prkd2/3*$^{\Delta CD4}$) mice, PLZF induction and iNKT cell generation were severely impaired, which were rescued by introduction of a PLZF transgene. We identified the transcription factor Ikaros as a substrate of PKD upon iTCR stimulation. Knock-in mice carrying a phosphorylation-defective mutant Ikaros (*Ikzf1*$^{S267/275A}$) exhibited an impairment of iNKT cell development, whereas conventional T cells were normal. In iNKT cells, Ikaros binds to the upstream region of the PLZF gene to induce its transcription. Mutant mice lacking the Ikaros-binding site (*Zbtb16*$^{\Delta IBS}$) generated fewer iNKT cells than WT mice. These results suggest that PKD links iTCRs to PLZF induction through Ikaros, thereby mediating iNKT cell development.

Introduction

Invariant natural killer T (iNKT) cells are a subset of innate-like T cells and are rapidly activated to exert effector functions by lipid antigens, such as α-galactosylceramide (α-GalCer), and exposure to cytokines (Brennan et al., 2013). While conventional T cells are selected by recognition of self-peptides presented on MHC molecules on thymic epithelial cells, development of iNKT cells requires interaction with $CD4^+CD8^+$ double-positive thymocytes through iTCR-CD1d and SLAM family molecules (Lantz and Bendelac, 1994; Godfrey and Berzins, 2007). Several self-derived lipid antigens (Birkholz and Kronenberg, 2015), including endogenous α-GalCer (Hosono et al., 2025), have been reported. Selected thymic iNKT cells undergo multiple maturation steps to differentiate into iNKT1, iNKT2, and iNKT17 subsets (Godfrey et al., 2010; Das et al., 2010; Constantinides and Bendelac, 2013; Wang and Hogquist, 2018).

Signaling through iTCR/SLAM plays an essential role in iNKT cell development, as evidenced by developmental arrest observed in mice lacking CD3ζ, Lck, Zap70, Lat, Slp-76, Vav, Itk, SAP, and Fyn (Godfrey et al., 2010). During iNKT cell development, iTCR engagement upregulates the transcription factor promyelocytic leukemia zinc finger (PLZF) (encoded by *Zbtb16*) (Chen et al., 2017), which is essential for the specification of unconventional T cells (Kovalovsky et al., 2008; Savage et al., 2008; Kreslavsky et al., 2009; Koay et al., 2016). PLZF induces multiple genes that determine characteristics of iNKT cell identity, such as effector functions and migration features (Mao et al., 2016). Although the transcription factors involved in PLZF upregulation have been reported (Seiler et al., 2012; Mao et al., 2017), the signaling pathway leading from the cell surface iTCR to the nucleus, which mediates the induction of PLZF, has not been fully understood.

Protein kinase D (PKD) comprises a serine/threonine kinase family classified as Ca^{2+}/calmodulin-dependent protein kinases (Rozengurt et al., 2005). PKDs are known to be localized in the nucleus upon stimulation (Rey et al., 2001; Irie et al., 2006) and phosphorylate nuclear substrates (Rozengurt et al., 2005). Among three similar isoforms (PKD1/2/3), only PKD2 and PKD3 are expressed in T cells and phosphorylated upon TCR stimulation (Irie et al., 2006; Matthews et al., 2010; Ishikawa et al., 2016). As the depletion of all PKD isoforms from double-negative thymocytes using *Lck*-Cre transgenic mice impaired positive selection of conventional T cells (Ishikawa et al., 2016), we sought to examine their precise roles in iNKT cell development using mouse models lacking PKD after this check point.

[1]Department of Molecular Immunology, Research Institute for Microbial Diseases, The University of Osaka, Suita, Japan; [2]Laboratory of Molecular Immunology, Immunology Frontier Research Center (IFReC), The University of Osaka, Suita, Japan; [3]Division of Cell Signaling, Institute of Advanced Medical Sciences, Tokushima University, Tokushima, Japan; [4]Genome Information Research Center, Research Institute for Microbial Diseases, The University of Osaka, Suita, Japan; [5]Department of Genetics, Hyogo Medical University, Nishinomiya, Japan; [6]Department of Immunology and Stem Cell Biology, Faculty of Medicine, Institute of Medical, Pharmaceutical and Health Sciences, Kanazawa University, Kanazawa, Japan; [7]Center for Infectious Disease Education and Research (CiDER), The University of Osaka, Suita, Japan; [8]Center for Advanced Modalities and DDS (CAMaD), The University of Osaka, Suita, Japan.

Correspondence to Sho Yamasaki: yamasaki@biken.osaka-u.ac.jp.

In this study, we found that the development of iNKT cells, but not conventional T cells, is severely impaired in *Cd4*-Cre–driven T cell–specific PKD-deficient mice. Proteomic analyses identified a novel PKD substrate, Ikaros, which contributes to PLZF induction. These results reveal the selective role of PKD in iNKT cell development.

Results

Loss of PKD results in defective iNKT cell generation

We have established mice lacking PKD in T cells by crossing PKD2$^{flox/flox}$ × PKD3$^{flox/flox}$ mice with *Lck*-Cre Tg mice (*Prkd2/3*$^{\Delta Lck}$). In the thymus of *Prkd2/3*$^{\Delta Lck}$ mice, both the proportion and number of iNKT cells were severely decreased as assessed by PBS-57 (α-GalCer analog)-loaded CD1d tetramer (Fig. 1 A). As *Prkd2/3*$^{\Delta Lck}$ mice impaired thymic selection of conventional T cells (Ishikawa et al., 2016), we also established *Cd4*-Cre–mediated T cell–specific PKD2/3-deficient (*Prkd2/3*$^{\Delta CD4}$) mice, which are deficient in PKD at later stages (Lee et al., 2001). Importantly, the total number of thymocytes as well as the percentages of CD4$^-$CD8$^-$ (DN), CD4$^+$CD8$^+$ (DP), CD4$^-$CD8$^+$ (8SP), and CD4$^+$CD8$^-$ (4SP) populations, were not affected in *Prkd2/3*$^{\Delta CD4}$ mice (Fig. S1 A and Fig. 1 B). Similarly, regulatory T cells and γδ T cells developed normally in *Prkd2/3*$^{\Delta CD4}$ mice (Fig. S1, B and C). However, the number and proportion of CD1d tetramer$^+$ iNKT cells were selectively decreased in *Prkd2/3*$^{\Delta CD4}$ mice (Fig. 1 C and Fig. S1 D). Moreover, innate-like T cells other than iNKT cells, such as mucosal-associated invariant T (MAIT) cells and γδ NKT cells (PLZF$^+$TCRVγ1.1$^+$Vδ6.3$^+$) (Kreslavsky et al., 2009), were decreased in *Prkd2/3*$^{\Delta CD4}$ mice (Fig. S1, E and F).

Since iNKT cells are selected by CD1d on DP thymocytes (Bendelac, 1995), we first examined surface molecules involved in antigen-presenting function on DP thymocytes. On the surface of *Prkd2/3*$^{\Delta CD4}$ DP thymocytes, CD1d and SLAM family molecules were normally expressed (Fig. 1 D). To further confirm which responding thymocytes or antigen-presenting cells are responsible for the iNKT cell defect in the absence of PKD, we complemented PKD-sufficient selecting DP thymocytes by 1:1 mixed bone marrow (BM) chimeras of WT and *Prkd2/3*$^{\Delta CD4}$ cells in T cell–deficient *Cd3e*$^{\Delta 5/\Delta 5}$ mice. In the recipient thymus at 10 wk after BM transplantation, *Prkd2/3*$^{\Delta CD4}$ BM cells did not give rise to iNKT cells even in the presence of WT DP thymocytes (Fig. 1 E), indicating that PKDs are intrinsically required for iNKT cell generation.

We suspected that the decreased number of iNKT cells in *Prkd2/3*$^{\Delta CD4}$ mice might be due to a survival defect in iNKT cells; however, ectopic expression of anti-apoptotic protein Bcl-2 did not restore the generation of iNKT cells (Fig. S1 G), suggesting that these defects cannot be explained solely by the viability of PKD-deficient iNKT cells.

Role of PKD at different stages of iNKT cell development

We next evaluated which stage of iNKT cell development and maturation is affected by loss of PKD. Within CD69$^-$ preselected DP thymocytes, the rearrangement of *Trav11* to *Traj18* to generate the invariant iNKT TCRα chain was normal in the absence of PKD (Fig. 2 A). Furthermore, the developmental defect was unlikely due to the low-affinity clonotypes used by iNKT TCR in *Prkd2/3*$^{\Delta CD4}$ mice, as top 5 clonotypes from WT and *Prkd2/3*$^{\Delta CD4}$ mice responded similarly to αGalCer-loaded CD1d (Fig. S2, A and B). We therefore examined the maturation stages of thymic iNKT cells by CD24, CD44, and NK1.1 expressions. CD1d tetramer$^+$ iNKT cell numbers at the stages 1, 2, and 3 were severely decreased, while the most immature, stage 0, iNKT cells (CD24$^+$CD44$^-$NK1.1$^-$) accumulated in *Prkd2/3*$^{\Delta CD4}$ mice (Fig. 2 B and Fig. S3 A), suggesting developmental arrest at this stage. This is also confirmed by the analysis of iNKT cell subsets assessed by the expressions of RORγt and PLZF (Lee et al., 2013). Consistent with the fact that stage 3 mainly consists of iNKT1 (Lee et al., 2013), the proportion of iNKT1 and IFNγ-producing iNKT cells were significantly reduced in *Prkd2/3*$^{\Delta CD4}$ mice (Fig. S3, B and C). Moreover, CD5 expression, which represents the summation of TCR signaling intensity (Azzam et al., 1998), was decreased in *Prkd2/3*$^{\Delta CD4}$ mice (Fig. 2 C), suggesting that iTCR signaling was impaired in the absence of PKD.

We further examined the gene signature of thymic iNKT cells using single-cell RNA- and TCR-sequencing (scRNA/TCR-seq). Consistent with the results of flow cytometric analysis, iNKT clonotype (*Trav11-Traj18*)-expressing cells in the iNKT1, but not iNKT17, cluster were decreased in *Prkd2/3*$^{\Delta CD4}$ cells (Fig. 2 D; and Fig. S3, D and E). Indeed, type 1 effector signature genes, such as *Gzma*, *Gzmb*, and *Klra9*, were severely downregulated in *Prkd2/3*$^{\Delta CD4}$ iNKT cells (Fig. S3 F). In addition, inhibitory molecules *Pdcd1* and *Lag3* were upregulated in PKD2/3-deficient iNKT cells (Fig. S3, F and G), suggesting that PKD2/3 may contribute to the maintenance of activation status of iNKT cells.

A similar trend was confirmed by the chromatin landscape revealed by single-cell ATAC-sequencing (scATAC-seq) (Fig. 2 E; and Fig. S3, H and I). iNKT cells are known to undergo silencing of CD8 during maturation to become CD4$^+$CD8$^-$ population (Engel et al., 2010). However, the chromatin condensation of *Cd8a* and *Cd8b1* loci (Fig. S3 I) and their downregulation (Fig. S3 F) were impaired in *Prkd2/3*$^{\Delta CD4}$ iNKT cells. Accordingly, aberrant CD8-expressing (CD4$^+$CD8$^+$ and CD4$^-$CD8$^+$) thymic iNKT cells emerged in *Prkd2/3*$^{\Delta CD4}$ mice (Fig. S3 J). One of the factors silencing CD8 locus is a transcription factor ThPOK (gene symbol, *Zbtb7b*) (Wang et al., 2008a), which determines CD4 lineage commitment (Muroi et al., 2008; Egawa and Littman, 2008). Consistent with this, the expression of ThPOK and chromatin accessibility of its promoter were reduced in *Prkd2/3*$^{\Delta CD4}$ iNKT cells (Fig. S3, F and I).

Role of PKD in PLZF induction

In thymic iNKT cells, the engagement of iTCR/SLAM induced rapid phosphorylation of PKD (Fig. 3 A). The same stimulation also upregulated the transcription of PLZF (Dutta et al., 2013), whereas it was impaired in the absence of PKD (Fig. 3 B). This was consistent with the analysis of iNKT cells during maturation stages in mice. PLZF protein was drastically upregulated from stage 0–1 and decreased to intermediate levels in stage 2 and 3 (Savage et al., 2008) (Fig. 3 C). However, in PKD-deficient mice, PLZF induction at stage 1 was severely impaired (Fig. 3 C). Other transcription factors involved in iNKT cell development (Seiler et al., 2012; Dose et al., 2009) were not strongly affected (Fig. S4 A). These results suggest that iTCR signaling leading to PLZF induction is uncoupled in the absence of PKD.

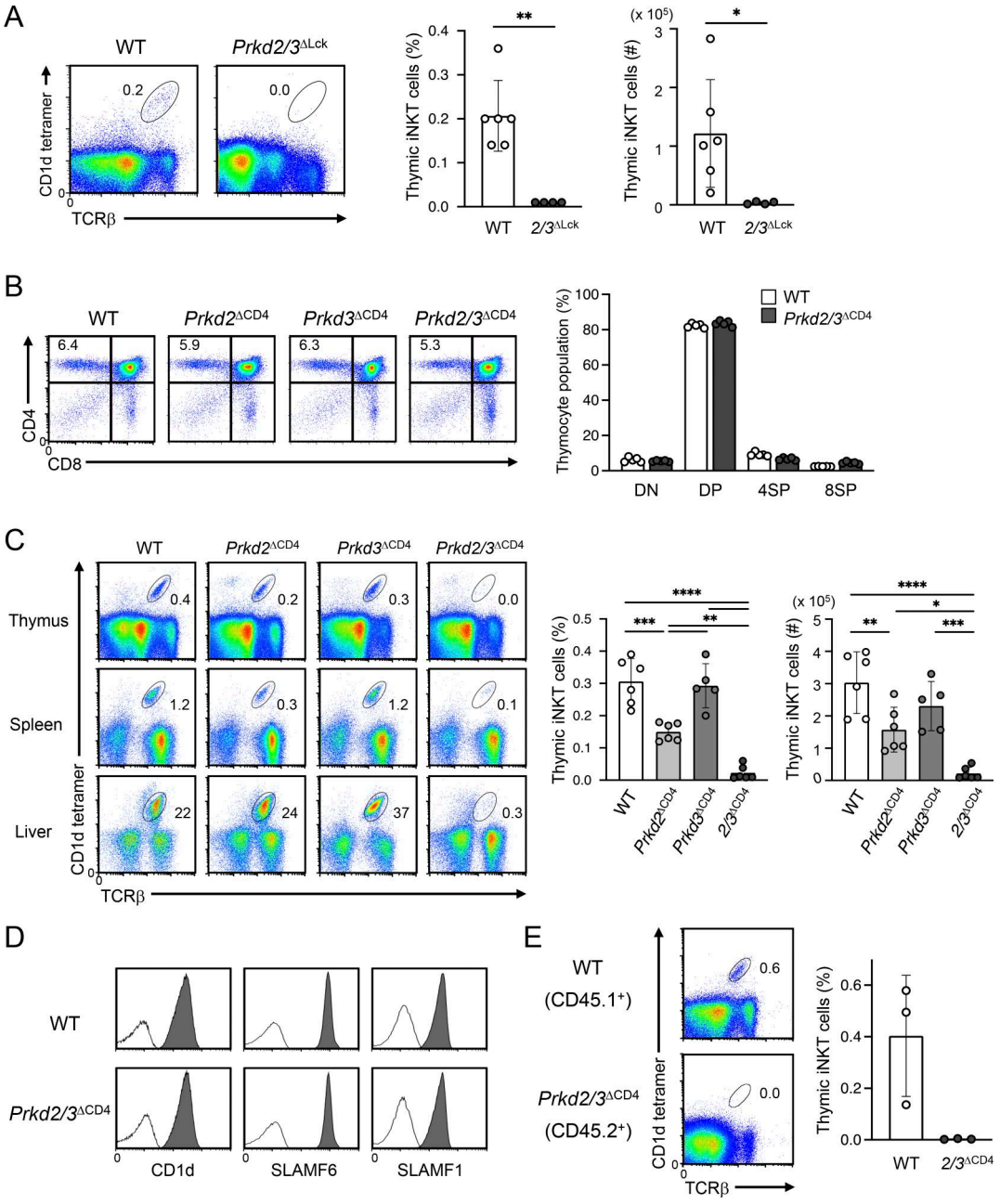

Figure 1. **PKD deficiency impairs iNKT cell generation. (A)** Representative FACS profiles of iNKT cells in the thymus from WT and *Lck*-Cre–mediated PKD-deficient mice (left) and bar graphs of the proportions (middle) and cell numbers (right) of iNKT cells in the thymus. Each symbol represents an individual mouse (n = 4–6), and the bar graphs indicate mean ± SD of proportions or cell numbers. **(B)** Representative FACS profiles of CD4 and CD8 expression on thymocytes (left) and bar graphs of the proportions of $CD4^-CD8^-$ (DN), $CD4^+CD8^+$ (DP), $CD4^+CD8^-$ (4SP), and $CD4^-CD8^+$ (8SP) cells (right) from WT, *Cd4*-Cre–mediated PKD2-deficient (*Prkd2*$^{\Delta CD4}$), PKD3-deficient (*Prkd3*$^{\Delta CD4}$), and PKD2/3-deficient (*Prkd2/3*$^{\Delta CD4}$) mice (n = 5). **(C)** Representative FACS profiles of iNKT cells in the thymus, spleen, and liver (left) and bar graphs of the proportions (middle) and cell numbers (right) of thymic iNKT cells from the indicated mouse strains (n = 5–6). **(D)** Expression of CD1d, SLAMF6, and SLAMF1 on DP thymocytes from WT and *Prkd2/3*$^{\Delta CD4}$ mice. Open histograms, no stain. Filled histograms, Ab stain. **(E)** Analysis of iNKT cell generation in the thymus of *Cd3e*$^{\Delta 5/\Delta 5}$ mice that were transferred with a mixture of Ly5.1$^+$ WT and Ly5.2$^+$ *Prkd2/3*$^{\Delta CD4}$ BM cells. 10 wk after BM transplantation (BMT), the proportion of iNKT cells within Ly5.1$^+$ or Ly5.2$^+$ thymocytes was analyzed. Representative FACS profiles (left) and bar graphs of the frequencies of thymic iNKT cells from three recipient mice (right) are shown. Each symbol represents an individual mouse, and the bar graphs indicate mean ± SD of proportions or cell numbers (A–C and E). Data are representative of two independent experiments (D and E). Statistical significance was determined by unpaired two-tailed Student's t test (A) or one-way ANOVA followed by Tukey's multiple comparison test (C). *P < 0.05, **P < 0.01, ***P < 0.001, and ****P < 0.0001.

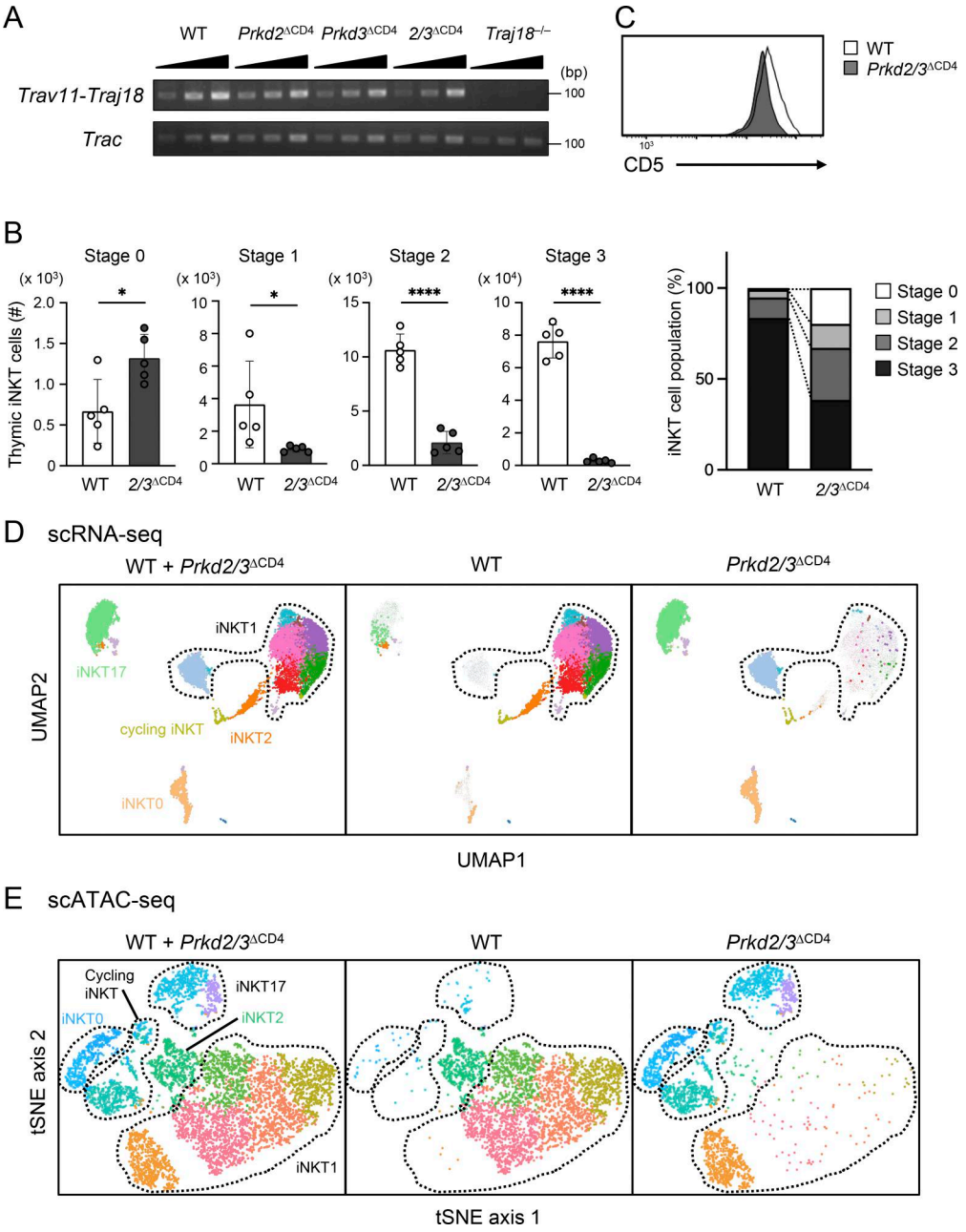

Figure 2. **Impaired thymic iNKT cell maturation in PKD-deficient mice. (A)** *Trav11-Traj18* (Vα14-Jα18) TCR rearrangements in CD69⁻ DP thymocytes from WT and the indicated PKD-deficient mice and in total thymocytes from *Traj18*$^{-/-}$ mice were detected by semiquantitative RT-PCR. mRNA expression of *Trac* (Cα) was analyzed as a control. Threefold serial dilutions of cDNAs were used as templates. **(B)** Analysis of maturation stages of WT and *Prkd2/3*$^{\Delta CD4}$ thymic iNKT cells. Bar graphs show the cell numbers (left) and average proportions (right) of CD1d tetramer⁺ iNKT cells at each stage. Each symbol represents an individual mouse (n = 5), and the bar graphs indicate mean ± SD of cell numbers (left). **(C)** Surface expression of CD5 on CD1d tetramer⁺ thymic iNKT cells from WT (open histogram) and *Prkd2/3*$^{\Delta CD4}$ mice (filled histogram). **(D)** UMAP projection of scRNA-seq data of *Trav11-Traj18*–expressing thymic iNKT cells from WT and *Prkd2/3*$^{\Delta CD4}$ mice. Within sorted CD1d tetramer⁺ cells, *Trav11-Traj18*–expressing cells were defined by simultaneous scTCR-seq analysis, sub-clustered by cell identity, and annotated by characteristic gene expression as shown in Fig. S3 D. **(E)** t-SNE analysis of scATAC-seq data of CD1d tetramer⁺ thymic iNKT cells from WT and *Prkd2/3*$^{\Delta CD4}$ mice. Cells were clustered by cell identity and annotated by features of chromatin accessibility as shown in Fig. S3 H. Data are representative of two (A) or three (C) independent experiments. Statistical significance was determined by unpaired two-tailed Student's t test (B). *P < 0.05 and ****P < 0.0001. Source data are available for this figure: SourceData F2.

To assess this possibility, we established PLZF transgenic (*Zbtb16* Tg) mice driven by the *Cd4* enhancer and promoter (Fig. S4 B). *Zbtb16* transgene restored both the proportion and number of iNKT cells in *Prkd2/3*$^{\Delta CD4}$ mice to levels comparable with WT mice (Fig. 3 D). Notably, we confirmed that *Zbtb16* Tg mice in a WT background did not show any iNKT cell increases as reported (Savage et al., 2008; Kovalovsky et al., 2010). These results suggest that defective PLZF induction contributes to the impaired iNKT cell development in the absence of PKD.

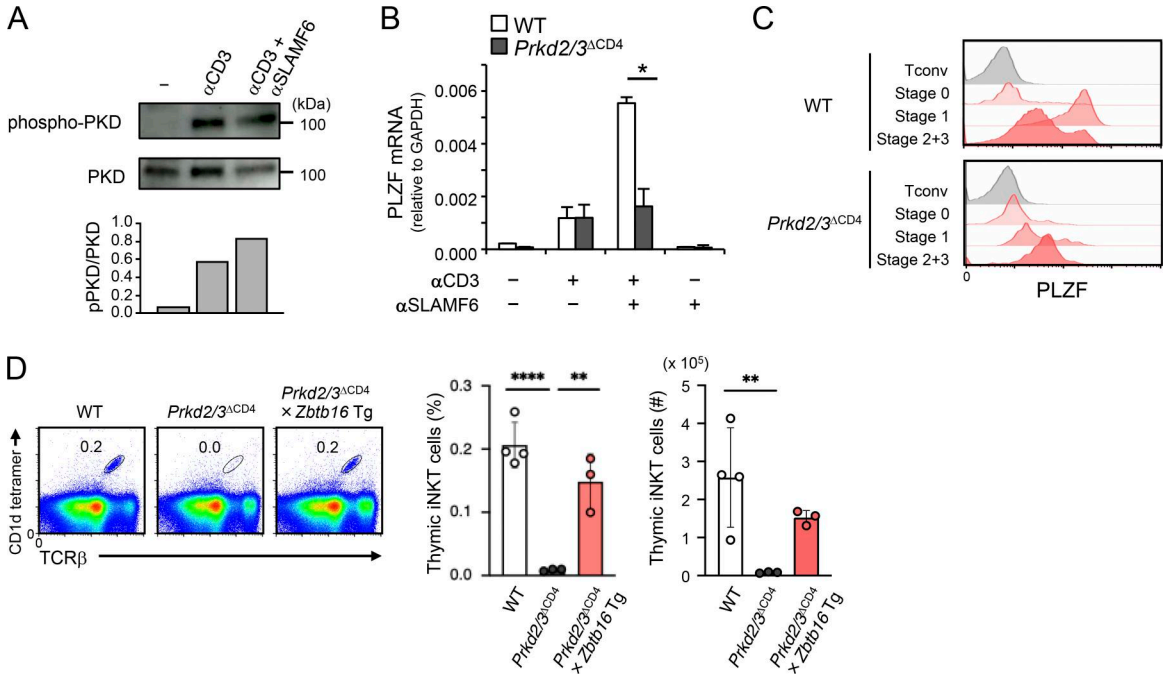

Figure 3. **PKD contributes to the induction of PLZF. (A)** Phosphorylation of PKD (pPKD) in thymic iNKT cells upon TCR stimulation by anti-CD3 cross-linking with or without anti-SLAMF6. Signals of phosphorylated PKD relative to those of total PKD were quantified using ImageJ software. **(B)** Real-time PCR analysis of PLZF mRNA expression levels in preselection DP thymocytes upon TCR stimulation by plate-bound anti-CD3, anti-SLAMF6 Abs, or both for 48 h. Results are presented as expression relative to GAPDH. **(C)** Protein expression of PLZF in CD1d tetramer⁺ thymic iNKT cells at each maturation stage. **(D)** Representative FACS profiles (left) and bar graphs of the proportions (middle) and cell numbers (right) of iNKT cells in the thymus from WT, *Prkd2/3*$^{\Delta CD4}$, and *Prkd2/3*$^{\Delta CD4}$ × *Zbtb16* Tg mice. Each symbol represents an individual mouse (n = 3–4). The bar graphs indicate mean ± SD of proportions or cell numbers. Data are representative of two (A and B) or three (C) independent experiments and presented as the mean ± SD of triplicate assays (B). Statistical significance was determined by unpaired two-tailed Student's t test (B) or one-way ANOVA followed by Tukey's multiple comparison test (D). *P < 0.05, **P < 0.01, and ****P < 0.0001. Source data are available for this figure: SourceData F3.

Ikaros is a PKD substrate in iNKT cells

To clarify the downstream signaling of PKD in iNKT cells, we established a PKD-deficient iNKT cell line and searched for PKD substrates by phosphoproteomic analysis using tandem mass tag (TMT) labeling. Despite lacking all PKD isoforms, TCR-induced Erk phosphorylation was not affected in these cells (Fig. 4 A), suggesting that PKD does not mediate all TCR signaling pathways. We therefore used these WT and PKD-deficient iNKT cell lines to search for PKD substrates. To assess this, we screened TCR-induced and PKD-dependent phosphopeptides using proteomics. Trypsin-digested peptides from unstimulated- and TCR-stimulated cells were labeled with different TMT reagents, mixed, phosphopeptides purified, and analyzed by mass spectrometry (Koshiba and Kosako, 2020). We identified 81 phosphopeptides that are increased in both a stimulation- and PKD-dependent manner, including 26 phosphopeptides possessing the PKD consensus phosphorylation motif (L/V/I/AxRxxpS/T) (Fig. 4 B). Among these 26 candidates, 14 molecules that are highly expressed in the thymus were evaluated by Phos-tag–based analysis. Ikaros and Rasal3 were directly phosphorylated by recombinant PKD2 and PKD3 *in vitro* (Fig. 4 C; and Fig. S5, A and B).

Phosphorylation-defective mutant Ikaros suppresses iNKT cell development

To examine the *in vivo* significance of PKD substrates phosphorylation in iNKT cell development, we established knock-in mice expressing phosphorylation-defective mutant of Ikaros (*Ikzf1*$^{S267/275A}$) and Rasal3 (*Rasal3*$^{S74/95A}$) (Fig. 4 D and Fig. S5 C). As phosphorylation sequences (LApSNVAK and SpSMPQK) are identical between Ikaros and Aiolos (Fig. 4 B), we also generated *Aiolos*$^{S260/268A}$ mice (Fig. S5 D). Among these mice, the percentage of iNKT cells in the thymus was reduced by half only in *Ikzf1*$^{S267/275A}$ mice (Fig. 4 E and Fig. S5, E–H). We also evaluated the ability of *Ikzf1*$^{S267/275A}$ thymocytes to give rise to iNKT cells under competitive condition. CD45.1⁺ WT and CD45.2⁺ *Ikzf1*$^{S267/275A}$ BM cells were mixed and transferred into T cell–deficient mice to analyze thymic iNKT cells after 15 wk. *Ikzf1*$^{S267/275A}$ cells could not efficiently develop into iNKT cells compared with WT thymocytes (Fig. 4 F), indicating that serine residues of Ikaros (Ser^{267}/Ser^{275}) are important for the development of iNKT cells. Of note, the development of conventional T cells and the expression of CD1d and SLAM family molecules were normal in *Ikzf1*$^{S267/275A}$ mice (Fig. S5, I–K).

Ikaros contributes to *Zbtb16* induction

We next evaluated the capacity of Ikaros to transactivate *Zbtb16* gene. To assess this, we searched for potential Ikaros-binding genomic regions by whole genome chromatin immunoprecipitation-sequencing (ChIP-seq) using a large number of thymic iNKT cells collected from iNKT cell–enriched (iNKT-iPS cell–derived) mice (Watarai et al., 2010; Ren et al., 2014). Preferential binding of Ikaros to promoter regions in the *Zbtb16* locus was detected in

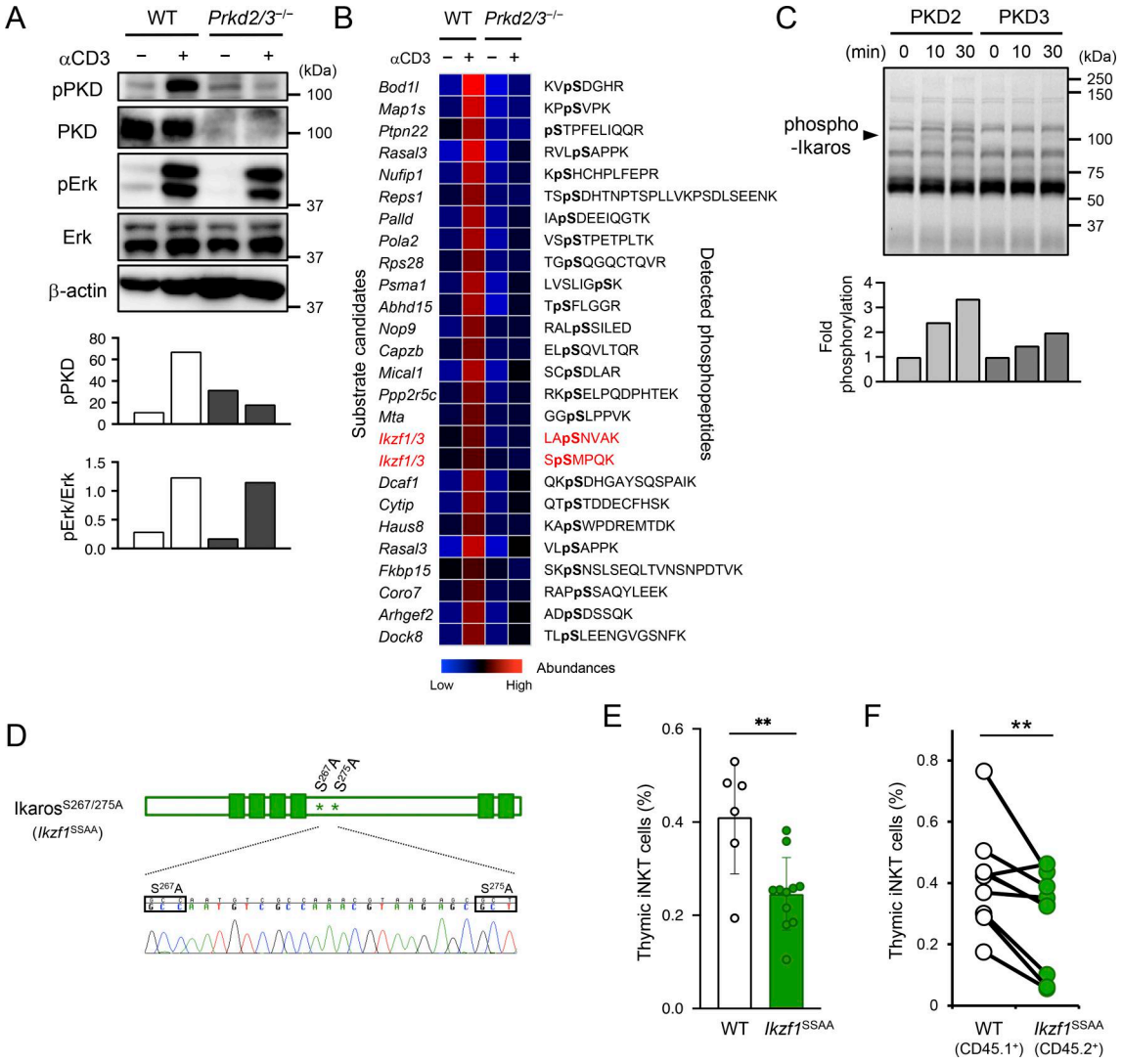

Figure 4. **Identification of PKD substrates in iNKT cells. (A)** Establishment of a PKD-deficient (*Prkd2/3*$^{-/-}$) iNKT cell line. Expression of PKD and phosphorylation of PKD and Erk upon TCR stimulation by anti-CD3 cross-linking were analyzed by western blotting. Erk and β-actin were detected as loading controls. Signals of phosphorylated PKD and phosphorylated Erk relative to total Erk expression were quantified using ImageJ software. **(B)** Proteomic analysis of phosphopeptides in unstimulated and TCR-stimulated WT and *Prkd2/3*$^{-/-}$ iNKT cell lines. The phosphopeptides that were increased in a stimulation- and PKD-dependent manner (with fold changes >1.5 and 2, respectively) and that also match the consensus motif for PKD substrates are shown. Abundances are presented as a heat map. **(C)** Phos-tag SDS-PAGE of GST-Ikaros after *in vitro* kinase assays in the presence of recombinant active PKD2 or PKD3 for the indicated times (upper). The arrowhead indicates the phosphorylated form of GST-Ikaros (phospho-Ikaros). Phosphorylated bands were quantified and presented as relative to those at 0 min. **(D)** Schematic protein structure of phosphorylation-defective mutant Ikaros (Ikaros$^{S267/275A}$) and genomic sequence analysis of *Ikzf1*$^{S267/275A}$ (*Ikzf1*^{SSAA}) knock-in allele. Locations of mutations are indicated by asterisks. Genomic DNAs were amplified using primers that crossover mutated bases, and the PCR products were cloned into a vector for sequencing. Six green boxes represent zinc finger domains. **(E)** Proportions of CD1d tetramer$^+$ iNKT cells in the thymus from WT and *Ikzf1*^{SSAA} mice. Each symbol represents an individual mouse (n = 6–11). The bar graphs indicate mean ± SD of proportions. **(F)** Analysis of iNKT cell generation in the thymus of *Cd3e*$^{Δ5/Δ5}$ mice that were transferred with a mixture of Ly5.1$^+$ WT and Ly5.2$^+$ *Ikzf1*^{SSAA} BM cells. 15 wk after BMT, the proportion of iNKT cells within Ly5.1$^+$ or Ly5.2$^+$ thymocytes was analyzed. Each line graph indicates an individual mouse (n = 9). Data are representative of two independent experiments (A and C). Statistical significance was determined by unpaired (E) or paired (F) two-tailed Student's t test. **P < 0.01. BMT, BM transplantation. Source data are available for this figure: SourceData F4.

thymic iNKT cells compared with total thymocytes (mostly conventional T cells), which was in sharp contrast to *Cd8a* locus (Fig. 5 A), an Ikaros target in conventional T cells (Harker et al., 2002). ChIP-qPCR analysis and luciferase reporter assay suggested the functional binding of Ikaros to the *Zbtb16* promoter (Fig. 5, B and C). The reporter activity was synergized in the presence of known *Zbtb16* regulator, Egr2, and dependent on the upstream region (−913 to −732), which overlaps with the ChIP-seq peak and includes Ikaros-binding motifs (Fig. 5, C and D).

Ikaros function may be mediated by binding partner(s) expressed in iNKT cells. We thus used proximity biotinylation to identify molecules that associate with Ikaros upon TCR stimulation. Using an iNKT cell line expressing TurboID-fused Ikaros, biotinylated peptides were purified and analyzed by mass spectrometry. Label-free quantification revealed that PKD2

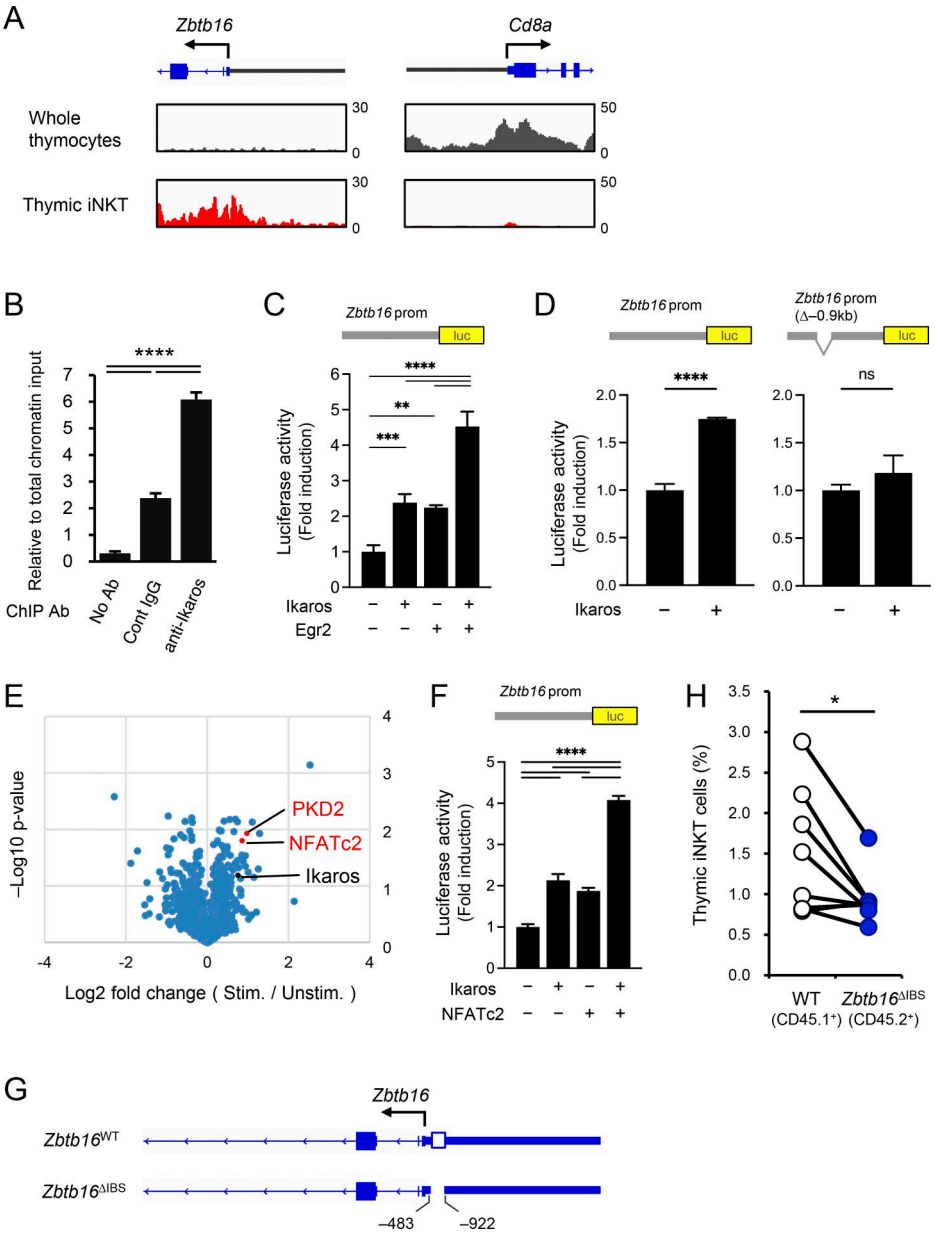

Figure 5. **Ikaros regulates transcription of *Zbtb16*. (A)** ChIP-seq analysis of Ikaros binding sites (IBSs) in WT total thymocytes and thymic iNKT cells from iNKT-iPS cell–derived mice. A part of the *Zbtb16* gene containing exons 1 and 2 (blue boxes) (left) or the *Cd8a* gene containing exons 1, 2, and 3 (right), and peaks associated with promoter region are shown. **(B)** ChIP-qPCR analysis of Ikaros binding to the promoter region of *Zbtb16* in thymocytes from WT mice. Data are presented as amplification relative to total chromatin input. **(C)** Luciferase activity in HEK293T cells transfected with a firefly luciferase (luc) expression plasmid driven by the *Zbtb16* promoter and transcription factors, Ikaros and Egr2. The activity is normalized by control *Renilla* luciferase activity and presented as activity relative to mock transfection. Schematic structure of a luc reporter construct is shown (upper). **(D)** Luciferase activity in HEK293T cells transfected with a firefly luciferase expression plasmid driven by the WT *Zbtb16* promoter (left) or a promoter lacking Ikaros-binding motifs (Δ –0.9 kb) (right) and Ikaros. Schematic structures of luc reporter constructs used in the assay are shown (upper). **(E)** A volcano plot of biotinylated peptides from an iNKT cell line expressing TurboID-Ikaros with or without TCR stimulation. Peptides derived from PKD2 and NFATc2 were detected as biotinylated peptides that increased upon TCR stimulation. **(F)** Luciferase activity in HEK293T cells transfected with a firefly luciferase expression plasmid driven by the *Zbtb16* promoter and transcription factors, Ikaros and NFATc2. **(G)** Schematic genomic structure of *Zbtb16*^{WT} and *Zbtb16*$^{\Delta IBS}$ alleles. The *Zbtb16* promoter and the region deleted in *Zbtb16*$^{\Delta IBS}$ allele (IBS) are shown. **(H)** Analysis of iNKT cell generation in the thymus of Rag1-deficient mice that were transferred with BM cells from Ly5.1$^+$ WT and Ly5.2$^+$ *Zbtb16*$^{\Delta IBS}$ mice. 15 wk after BMT, the proportion of iNKT cells within Ly5.1$^+$ or Ly5.2$^+$ thymocytes was analyzed. Each line graph indicates an individual mouse (n = 8). Data are presented as the mean ± SD of triplicate assays and representative of two independent experiments (B–D and F). Statistical significance was determined by one-way ANOVA, followed by Tukey's multiple comparison test (B, C, and F), unpaired (D) or paired (H) two-tailed Student's t test. ns, not significant. *P < 0.05, **P < 0.01, ***P < 0.001, and ****P <0.0001. BMT, BM transplantation.

associated with Ikaros upon TCR stimulation (Fig. 5 E), in accordance with the observation that Ikaros is a PKD substrate (Fig. 4, B and C). In addition, NFATc2 was identified as another Ikaros-interacting protein upon TCR stimulation. This interaction may promote Ikaros function, as co-expression of NFATc2 increased the transcriptional activity of Ikaros (Fig. 5 F).

Finally, to investigate the role of the Ikaros-binding site (IBS) in the *Zbtb16* promoter, we established mice in which the upstream region (−922 to −483) of the *Zbtb16* gene was deleted (*Zbtb16*$^{\Delta IBS}$) (Fig. 5 G and Fig. S5 L). In competitive BM chimeras using Rag1-deficient mice as recipients, CD45.2$^+$ *Zbtb16*$^{\Delta IBS}$ BM cells generated fewer thymic iNKT cells than CD45.1$^+$ WT cells (Fig. 5 H). These results suggest that the IBSs within the *Zbtb16* promoter are required for iNKT cell development.

Discussion

In this study, we showed a role of PKD family kinases in iNKT cell development. T cell lineage expresses abundant PKD2, less PKD3, and no PKD1 (Ishikawa et al., 2016). PKD2 or PKD3 single deficiency (*Prkd2*$^{\Delta CD4}$ or *Prkd3*$^{\Delta CD4}$) and PKD2/3 double haploinsufficiency (*Prkd2/3*$^{flox/+}$ × *Cd4*-Cre) had a small effect on the iNKT cell number, indicating that PKD2 and PKD3 are functionally redundant. However, the expression level in thymocytes (Ishikawa et al., 2016) and enzyme activity of PKD2 were higher than those of PKD3, which is consistent with the more substantial effect of PKD2 deficiency compared with PKD3 deficiency.

The reason why PKD is selectively required for iNKT cell development is unknown, but agonist selection through iTCR may largely be dependent on PKD compared with peptide-induced selection of conventional T cells. It is possible that iTCR and SLAM cooperatively regulate PKD for postselection proliferation and functional maturation of iNKT cells, including PLZF induction. Indeed, stimulation via iTCR and SLAM6 synergistically upregulated PLZF in a PKD2/3-dependent manner. Since transgenic expression of PLZF in *Prkd2/3*$^{\Delta CD4}$ mice restored iNKT cell development, the impairment of iNKT cell development in *Prkd2/3*$^{\Delta CD4}$ mice is mainly due to insufficient induction of PLZF. Further investigation is needed to clarify how the dose and the timing of PLZF induction contribute to iNKT cell development and subset differentiation. In addition to other reported transcription factors regulating PLZF (Seiler et al., 2012; Mao et al., 2017; Gioulbasani et al., 2020), the present study identified Ikaros as a critical mediator of PKD-dependent PLZF induction based on the following findings: (1) Ikaros is a direct substrate of PKD, (2) Ikaros is associated with PKD2 upon TCR stimulation, (3) *Ikzf1*$^{S267/275A}$ knock-in mice are impaired in iNKT cell development, (4) Ikaros binds to the PLZF promoter and activates transcription, and (5) deletion of the PLZF promoter region (*Zbtb16*$^{\Delta IBS}$ mice) impaired iNKT cell development.

Ikaros is a pleiotropic transcriptional regulator of lymphocyte differentiation and function (Kastner and Chan, 2024). Its mutation or deficiency causes dysregulated lymphoid system ranging from malignancy to immunodeficiency (Boast et al., 2021). In T cells, Ikaros regulates β-selection, positive selection, and peripheral activation (Winandy et al., 1999; Avitahl et al., 1999; Bernardi et al., 2021), mainly as a transcriptional suppressor. Such defects were not observed in *Ikzf1*$^{S267/275A}$ knock-in mice, suggesting that PKD-mediated posttranslational modification of Ikaros confers a unique function(s) to specific cell types, such as unconventional T cells. Although PKD is known to shuttle between cytoplasm and nucleus depending on cell status (Rey et al., 2001; Irie et al., 2006), we still do not know where Ikaros is phosphorylated and whether the phosphorylation regulates its subcellular localization (Uckun et al., 2012). Alternatively, iTCR-induced Ikaros phosphorylation may alter its binding partners; NFATc2 may be one of the candidates (Fig. 5 E) (Gabriel et al., 2016). Overall, this study proposes a previously unappreciated function of Ikaros in regulating the iNKT cell developmental program and, perhaps, agonist selection of unconventional T cells. Indeed, PLZF is required for the generation of other unconventional T cells, such as γδ NKT cells (PLZF$^+$TCRVγ1$^+$Vδ6.3$^+$) and MAIT cells (Kreslavsky et al., 2009; Koay et al., 2016), both of which were decreased in *Prkd2/3*$^{\Delta CD4}$ mice.

During iNKT cell development, TCR signal strength can influence iNKT subsets; iNKT2 and iNKT17 require strong TCR signal (Zhao et al., 2018; Tuttle et al., 2018). Expression levels of CD5, which reflect the sum of TCR signaling, were lower in iNKT cells from *Prkd2/3*$^{\Delta CD4}$ mice. Fewer iNKT2 in *Prkd2/3*$^{\Delta CD4}$ mice is therefore likely due to the reduced iTCR signaling. However, iNKT17 cells were increased in *Prkd2/3*$^{\Delta CD4}$ mice, which may be explained by the lower expression of ThPOK that suppresses iNKT17 development (Engel et al., 2012; Enders et al., 2012). Lower ThPOK may also cause CD8 derepression (also called redirection or re-expression) (Muroi et al., 2008; Wang et al., 2008b; Egawa and Littman, 2008) of iNKT cells in *Prkd2/3*$^{\Delta CD4}$ mice. In *Cd4*-Cre–driven ThPOK-deficient mice, a similar CD8 derepression of iNKT cells (i.e., generation of CD8$^+$ iNKT cells) was observed (Liu et al., 2014). The low expression of ThPOK might be partly due to the loss of PLZF as reported (Gleimer et al., 2012). Indeed, aberrant "redirected" CD8$^+$ iNKT cells in *Prkd2/3*$^{\Delta CD4}$ mice disappeared with transgenic expression of PLZF (Fig. S4 C).

The residual iNKT cells developed in the absence of PKD might be selected due to the compensatory acquisition of TCR with high affinity to CD1d and antigens, as is frequently observed in conventional T cells (Takeuchi et al., 2020). However, reconstitution of reporter cells with frequent iNKT TCRαβ clonotypes from WT or *Prkd2/3*$^{\Delta CD4}$ mice resulted in similar dose-dependent reactivity to α-GalCer–presenting CD1d, suggesting that such compensation resulting from variation in the TCR affinity spectrum is unlikely to occur in invariant TCRs (Karnaukhov et al., 2024). We recently detected the most potent antigen, α-GalCer, in the thymus (Hosono et al., 2025). It may support a "simple" selection process of iNKT cells via the interaction of "invariant" TCR versus "less diverse" antigen, which does not depend on the strict monitoring of mutual affinity, unlike conventional T cells (Bortoluzzi et al., 2021; Karnaukhov et al., 2024).

Taken together, PKD is a critical mediator in dictating transcriptional programs regulating iNKT cell generation and in conferring functional features to iNKT cell subsets.

Materials and methods

Mice

PKD2-floxed and PKD3-floxed mice (Ishikawa et al., 2016) were generated as described previously. *Bcl2* Tg mice (Kondo et al., 1997) were provided by J. Domen (The Children's Mercy Hospital, Kansas City, MO, USA) by the courtesy of K. Ikuta (Kyoto University, Kyoto, Japan). *Cd3e*$^{\Delta 5/\Delta 5}$ (Malissen et al., 1995) mice were provided by B. Malissen (Aix Marseille Universite UM2, Marseille, France); *Traj18*$^{-/-}$ mice (Cui et al., 1997) were provided by M. Taniguchi (RIKEN, Yokohama, Japan). Previously, iNKT-iPS cell–derived mice were generated using iPS cells with rearranged *Trav11-Traj18* in TCRα locus, which were established by the retroviral transduction of Oct3/4, Sox2, Klf4, and c-Myc into iNKT cells (Watarai et al., 2010; Ren et al., 2014). However, the mice were easily cancerous due to the insertion of retroviral vectors into the genome. Here, we have regenerated iNKT-iPS cells and its derived mice without any mutations and insertions using episomal vectors containing the autonomously replicating sequence. Tg mice expressing PLZF under *Cd4* enhancer and promoter were established by using a vector (Taniuchi et al., 2002) provided by I. Taniuchi (RIKEN). For the generation of *Ikzf1*$^{S267/275A}$ and *Ikzf3*$^{S260/268A}$ knock-in mice, crRNA (gRNA sequence; 5′-AGGCATAGAGCTCTTACGTT-3′ or 5′-GGACAGATT AGCAAGCAATG-3′), tracrRNA, donor ssDNA with S267/275A or S260/268A mutation, and Cas9 proteins were electroporated into fertilized eggs. For the generation of *Rasal3* $^{S74/95A}$ knock-in mice, a targeting construct bearing S74/95A mutation was used for homologous recombination in C57BL/6-derived ES cells, and the *Neo* cassette was deleted after germline transmission. *Zbtb16*$^{\Delta IBS}$ mice were generated by electroporation of crRNA (gRNA sequences; 5′-CGTTTCCCAAGTCCCAAACC-3′ and 5′-AGA GCGCACGGGCTCTGCCA-3′), tracrRNA, donor ssDNA with deletion of *Zbtb16* promoter region (−922 to −483), and Cas9 proteins in fertilized eggs. Male and female mice of 7–12 wk of age with C57BL/6 background were used for all experiments. Littermates or age- and sex-matched WT mice maintained in the same breeding room were used as control mice. All mice were maintained in filter-air laminar-flow enclosures and given standard laboratory food and water *ad libitum*. All animal experiments were approved by the Animal Care and Use Committee of the Research Institute for Microbial Diseases, The University of Osaka.

Cells

iNKT cell line, DN32.D3 cells (Bendelac et al., 1995), were kindly provided by Y. Kinjo (Jikei University School of Medicine, Tokyo, Japan). Mouse T cell hybridoma lacking TCR expression (Matsumoto et al., 2021) was kindly provided by H. Arase (The University of Osaka, Suita, Japan). These cells were maintained in RPMI1640 medium (Sigma-Aldrich) supplemented with 10% FBS (Sigma-Aldrich and Capricorn Scientific), 100 U/ml penicillin, 10 µg/ml streptomycin, and 50 µM 2-mercaptoehthanol. HEK293T cells and Phoenix retroviral packaging cells were maintained in DMEM medium (Sigma-Aldrich) supplemented with 10% FBS, 100 U/ml penicillin, 10 µg/ml streptomycin, and 50 µM 2-mercaptoehthanol.

For establishment of PKD-deficient iNKT cell line, DN32.D3 was introduced with pX330-PKD2 sgRNA (5′-GCCGGGGAGTCC TGCGGGAT-3′), pX330-PKD3 sgRNA (5′-ACGAGAGAGTGTTAC CATCG-3′), and neomycin resistant gene-expressing vector using electroporator NEPA21 (NEPAGENE). *Prkd2/3*$^{-/-}$ cells were selected by G418 treatment followed by limiting dilution. Loss of protein expression was confirmed by western blotting.

Reagents

For cell surface staining, anti-TCRβ (H57-597), anti-CD45R/B220 (RA3-6B2), anti-CD45.1 (A20), anti-CD45.2 (104), anti-SLAMF6 (330-AJ), anti-SLAMF1 (TC15-12F12.2), anti-CD4 (RM4-5), anti-CD8 (53–6.7), anti-TCRγδ (GL3), anti-CD24 (M1/69), anti-CD44 (1M7), anti-NK1.1 (PK136), anti-TCRVγ1.1 (2.11), anti-TCRVδ6.3 (C504.17C), anti-CD5 (53–7.3), anti-CD3ε (145-2C11), and anti-CD69 (H1.2F3) antibodies (Abs) were purchased from BioLegend, and anti-CD1d (1B1) and anti-CD25 (PC61) Abs were from BD Biosciences. T-select mouse CD1d tetramer was purchased from MBL. PBS-57–loaded mouse CD1d tetramer and 5OP-RU–loaded MR1 tetramer were provided by NIH Tetramer Core Facility. For intracellular staining, anti-PLZF (R17-809) and anti-RORγt (Q31-378) were obtained from BD Biosciences, anti-Foxp3 (FJK-16S), anti-IFNγ (XMG1.2), anti–IL-4 (11B11), anti–T-bet (eBio4B10), and anti-Egr2 (erongr2) Abs were from eBioscience, anti–IL-17 (TC11-18H10.1) was from BioLegend, and anti–c-Myc (E5Q6W) was from Cell Signaling Technology. For Western blotting, anti-pErk1/2 (cat#4379, 1:2,000), anti-Erk (cat#9102, 1:1,000), anti-PKD3 (cat#5655, 1:4,000), and anti–β-actin (cat#4970, 1:1,000) Abs were obtained from Cell Signaling Technology. Anti-PKD1 (cat#NBP1-98311, 1:1,000) and anti-PKD2 (cat#NB100-636, 1:500) Abs were from Novus Biologicals. Anti-phospho PKD Ab was raised as described previously (Ishikawa et al., 2016). Anti-Ikaros (D6N9Y) Ab from Cell Signaling Technology was used for ChIP-seq. Anti-Ikaros (cat#ab229275) Ab used for ChIP-qPCR was purchased from abcam. For iNKT TCR stimulation, anti-CD3ε (145-2C11) and secondary Ab goat anti-Hamster IgG Ab (MP Biomedicals) or α-GalCer (KRN7000) from Kyowa Hakko Kirin Co., Ltd were used.

Flow cytometry

Cells were isolated from thymus, spleen, and liver. For iNKT stages and subsets analysis, thymic iNKT cells were enriched by staining with APC-labeled PBS-57–loaded mouse CD1d tetramer and anti-APC microbeads followed by magnetic separation. Thymic MAIT cells were enriched using APC-labeled 5-OP-RU–loaded mouse MR1 tetramer in the same manner. For the analysis of liver iNKT cells, the liver was perfused with PBS, and liver mononuclear cells were isolated by Percoll density gradient centrifugation. Cells were stained with fluorescent-labeled Abs and analyzed by Gallios (Beckman Coulter) or Attune NxT (Thermo Fisher Scientific), followed by data analysis using FlowJo software (BD Biosciences). For intracellular staining of transcription factors, cells were stained with Abs for cell surface staining, fixed, and permeabilized using Foxp3/transcription factor staining buffer set (eBioscience), followed by staining of Foxp3, PLZF, RORγt, T-bet, Egr2 and c-Myc. For intracellular staining of cytokines, enriched thymic iNKT cells were stimulated with 50 µg/ml PMA and 1 µM ionomycin for 4 h. 10 µg/ml Brefeldin A was added 1 h after the start of stimulation. Cells

were fixed and permeabilized using the same buffer set and stained for IFNγ, IL-4, and IL-17 and then analyzed by FACSCalibur (BD Biosciences) or Attune NxT (Thermo Fisher Scientific).

BM chimeras

BM cells were isolated from the femur, fibula, and pelvis of donor mice. 5×10^6 cells from CD45.1$^+$ WT and CD45.2$^+$ *Prkd2/3*$^{\Delta CD4}$, CD45.2$^+$ *Ikzf1*$^{S267/275A}$, CD45.2$^+$ *Rasal3*$^{S74/95A}$, CD45.2$^+$ *Ikzf3*$^{S260/268A}$, or CD45.2$^+$ *Zbtb16*$^{\Delta IBS}$ mice were mixed at 1:1 ratio and injected intravenously into 8 Gy-irradiated *Cd3e*$^{\Delta 5/\Delta 5}$ mice or 4 Gy-irradiated Rag1-deficient mice. After 10–15 wk, recipient mice were analyzed for development of iNKT cells.

Detection of *Trav11-Traj18* gene rearrangement

CD69$^-$ DP thymocytes were isolated from thymus using FACSAria (BD Biosciences), and cDNA was obtained using Sepasol-RNA I Super G (Nacalai Tesque) and ReverTra Ace qPCR RT master mix (TOYOBO). Semiquantitative RT-PCR was conducted using Blend Taq polymerase (TOYOBO) and the following primers: *Trav11-Traj18* (F: 5′-GGATGACACTGCCACCTACA-3′, R: 5′-CTGAGTCCCAGCTCCAAAA-3′); *Trac* (F: 5′-TTCAAAGAGACC AACGCCAC-3′, R: 5′-TTCAGCAGGAGGATTCGGAG-3′).

Immunoblotting

A single-cell suspension of thymocytes was incubated overnight to extinguish the TCR signals. Thymic iNKT cells were purified by negative sorting using NK1.1$^+$ iNKT cell isolation kit (Miltenyi) to avoid possible triggering of TCR signals during the purification process using CD1d tetramer. Enriched iNKT cells were stained with 10 μg/ml biotinylated anti-CD3 (145-2C11) and anti-SLAMF6 (330-AJ) Abs at 4°C for 30 min, washed twice with cold medium, and then cross-linked by 100 μg/ml streptavidin at 37°C for 2 min. After stimulation, cells were rapidly transferred on ice and added with cold HEPES-buffered saline for washing. Then, cells were lysed in lysis buffer containing 1% Nonidet P-40, 1 mM PMSF, and protease inhibitor cocktail, and analyzed by western blotting. For the stimulation of DN32.D3 iNKT cell line, cells were stained with 10 μg/ml anti-CD3 Ab (145-2C11) and cross-linked with 100 μg/ml goat anti-Hamster IgG for 5 min. Mixture of anti-PKD1, anti-PKD2, and anti-PKD3 Abs were used for detection of all PKD isoforms. Signals were quantified using ImageJ software.

Quantitative real-time PCR

CD69$^-$ preselection DP thymocytes were stimulated by plate-bound anti-CD3 and anti-SLAMF6 Abs, and cDNA was obtained using Sepasol-RNA I Super G (Nacalai Tesque) and ReverTra Ace qPCR RT master mix (TOYOBO). Quantitative real-time PCR was conducted with THUNDERBIRD SYBR qPCR Mix (TOYOBO) using QuantStudio 5 (Thermo Fisher Scientific). Following primer sets were used: PLZF (F: 5′-ATGAAGGCTGAGAGCCGCCC-3′, R: 5′-TTC CGCAGAGTTCACACCCGT-3′); GAPDH (F: 5′-TGGTGAAGGTCG GTGTGAAC-3′, R: 5′-CCATGTAGTTGAGGTCAATGAAGG-3′).

Single cell–based transcriptome, TCR repertoire, and chromatin accessibility analysis

Thymic iNKT cells were stained with PBS-57–loaded mouse CD1d tetramer and enriched by magnetic beads cell sorting, followed by purification of CD1d-tetramer$^+$TCRβ$^+$ cells using cell sorter SH800S (SONY). For scRNA/TCR-seq, ∼3×10^4 cells were loaded into Chromium microfluidic chips to generate single-cell gel bead-in-emulsion using Chromium Controller (10x Genomics). Library preparation for scRNA-seq and scTCR-seq were performed simultaneously using the Chromium Next GEM Single Cell 5′ Reagent Kits v1.1 (10x Genomics) according to the manufacturer's protocol. The following reagent kits were used: Chromium Next GEM Single Cell 5′ Library & Gel Bead Kit v1.1 (PN-1000165), Chromium Next GEM Chip G Single Cell Kit (PN-1000120), Chromium Single Cell V(D)J Enrichment Kit, Human T Cell (PN-1000005), and Chromium i7 Multiplex Kit N, Set A (PN-1000084). Libraries were sequenced on an Illumina NovaSeq 6000 as paired-end mode (read 1, 28 bp; read 2, 91 bp). The raw reads were processed by Cell Ranger 3.1.0 (10x Genomics). Gene expression–based clustering was visualized by BBrowserX (BioTuring) and Loupe V(D)J Browser 5.1.0 (10x Genomics). For UMAP analysis of scRNA-seq data of iNKT cells in sorted cells, *Trav11-Traj18*–expressing cells were selected based on scTCR-seq data and sub-clustered.

For scATAC-seq analyses, nuclei were isolated from purified 6–70 × 10^4 iNKT cells according to the manufacturer's protocol (10x Genomics). Library preparation for scATAC-seq was performed using the Chromium Next GEM Single Cell ATAC Reagent Kits v1.1 (10x Genomics), including Chromium Next GEM Single Cell ATAC Library & Gel Bead Kit v1.1 (PN-1000175), Chromium Next GEM Chip H Single Cell Kit (PN-1000162), and Chromium i7 Multiplex Kit N, Set A (PN-1000084), following the manufacturer's protocol (CG000209; Rev C). Sequencing was conducted on a DNBSEQ-G400RS (MGI Tech Co., Ltd.) platform with paired-end mode. The sequencing configuration included 90 bp for Read 1, 100 bp for Read 2, and 16 bp for the 10x Barcode. Data analysis was performed using Cell Ranger ATAC v1.2.0 with the refdata-cellranger-atac-mm10–1.2.0 reference genome. Chromatin accessibility-based clustering was visualized by Loupe Browser 7.0.1 (10x Genomics).

TMT-based phosphoproteomic analysis

For TMT-based phosphoproteomic analysis, we established a PKD-deficient DN32.D3 iNKT cell line to obtain 10^8 iNKT cells as described above. WT and PKD-deficient cells were treated with 10 μg/ml anti-CD3 Ab and cross-linked with 100 μg/ml goat anti-Hamster IgG for 5 min. Cells were washed with ice-cold HEPES saline and lysed with Guanidine-HCl buffer (6 M guanidine-HCl, 100 mM Tris-Cl, pH 8.0, and 2 mM dithiothreitol). The lysates were dissolved through heating and sonication, followed by centrifugation at 20,000 × *g* for 15 min at 4°C. The supernatants were reduced in 5 mM dithiothreitol at room temperature for 30 min and alkylated in 27.5 mM iodoacetamide at room temperature for 30 min in the dark. Proteins (250 μg each) were purified using methanol–chloroform precipitation and solubilized with 25 μl of 0.1% RapiGest SF (Waters) in 50 mM triethylammonium bicarbonate. The proteins were digested with 2.5 μg of Trypsin/Lys-C mix (Promega) for 16 h at 37°C. Peptide concentrations were determined using a Pierce quantitative colorimetric peptide assay (Thermo Fisher Scientific). The digested peptides (150 μg each) were labeled with 0.2 mg

of TMT-10plex reagents (Thermo Fisher Scientific) for 1 h at 25°C. After the reaction was quenched with hydroxylamine, all TMT-labeled samples were pooled, acidified with trifluoroacetic acid (TFA), and subjected to the High-Select Fe-NTA phosphopeptide enrichment kit (Thermo Fisher Scientific). The eluates were acidified and fractionated using the Pierce High pH reversed-phase peptide fractionation kit (Thermo Fisher Scientific) according to the manufacturer's instructions. Nine fractions were collected using 5%, 7.5%, 10%, 12%, 14%, 16%, 18%, 20%, and 50% acetonitrile (ACN). Each fraction was evaporated using a SpeedVac concentrator and dissolved in 0.1% TFA.

Liquid chromatography tandem mass spectrometry (LC-MS/MS) analysis of the resulting peptides was performed on an EASY-nLC 1200 UHPLC system connected to a Q Exactive Plus mass spectrometer through a nanoelectrospray ion source (Thermo Fisher Scientific). The peptides were separated on a C18 reversed-phase column (75 µm × 150 mm; Nikkyo Technos) with a linear gradient of 4–20% ACN for 0–150 min and 20–32% ACN for 150–190 min, followed by an increase to 80% ACN for 10 min and a final hold at 80% ACN for 10 min. The mass spectrometer was operated in data-dependent acquisition mode with the top 10 MS/MS method. MS1 spectra were measured with a resolution of 70,000, an automatic gain control (AGC) target of 3e6, and a mass range of 375–1,400 *m/z*. HCD MS/MS spectra were acquired at a resolution of 35,000, AGC target of 1e5, isolation window of 0.7 *m/z*, maximum injection time of 100 ms, and normalized collision energy of 32. The dynamic exclusion was set at 30 s. Raw data were directly analyzed against the Swiss-Prot database restricted to *Mus musculus* using Proteome Discoverer 2.2 (Thermo Fisher Scientific) with the Mascot search engine for identification and TMT quantification. The search parameters were as follows: (1) trypsin as an enzyme with up to two missed cleavages, (2) precursor mass tolerance of 10 ppm, (3) fragment mass tolerance of 0.02 Da, (4) TMT of lysine and peptide N terminus and carbamidomethylation of cysteine as fixed modifications, and (5) oxidation of methionine, deamidation of asparagine and glutamine, and phosphorylation of serine, threonine, and tyrosine as variable modifications. Peptides were filtered at a false-discovery rate (FDR) of 1% using the percolator node.

Preparation of GST-fused Ikaros and *in vitro* kinase assay

cDNA of Ikaros, Aiolos, and truncated form of Rasal3 coding 1–500 amino acid residues was cloned into pGEX-6P-1 vector (Cytiva). The vector was transformed into *Escherichia coli* BL21-CodonPlus(DE3)-RIPL (Agilent Technologies), and GST-fused protein was purified using glutathione agarose (Pierce). For *in vitro* kinase assay, 6 µg GST-fused protein was incubated with 100 ng active PKD2 or PKD3 (Carna Bioscience) in 20 µl kinase buffer (1 mM ATP, 15 mM $MgCl_2$, and 20 mM Tris-HCl, pH 7.5) for 0–30 min at 30°C. The reaction was stopped by addition of sample buffer, followed by heating at 95°C for 10 min. Samples were subjected to Phos-tag SDS-PAGE using 7.5% acrylamide gel containing 50 µM Phos-tag acrylamide (Wako chemicals) and 100 µM $MnCl_2$. The gel was stained with Coomassie brilliant blue, and signals were quantified using ImageJ software.

ChIP-seq

To obtain sufficient number of primary iNKT cells required for ChIP-seq analysis, we used CD1d tetramer–purified thymic iNKT cells from iNKT-iPS cell–derived mice that have abundant thymic iNKT cells. Total thymocytes from WT mice and CD1d tetramer–purified thymic iNKT cells from iNKT-iPS cell–derived mice were immediately frozen by liquid nitrogen. Frozen cells were sent to active motif for ChIP-seq analysis. Active motif fixed cells, prepared chromatin, performed ChIP reactions, library generation, and barcoding for next-generation sequencing and data analysis. Spike-in of *Drosophila* chromatin was performed before ChIP for normalization. 30 µg of chromatin and 30 µl of anti-Ikaros Ab were used for the ChIP reaction, and the reaction was validated by qPCR. Library generation, library quality check, and barcoding were performed, and then next-generation sequencing was done using Illumina NextSeq 500. As an input, equal amounts of unprecipitated genomic DNA from each sample were used to generate a next-generation sequencing libraries and sequenced in parallel with the ChIP-seq samples. The 75-nt single-end (SE75) sequence reads were mapped to the genome using the BWA algorithm (v0.7.12, bwa aln/samse with default settings). Data were visualized with Integrative Genomics Viewer (IGV v2.4.3).

ChIP-qPCR

Total thymocytes were suspended in PBS containing 1 mM $MgCl_2$, and 2 mM disuccinimidyl glutarate was added for cross-linking. After incubation, cells were fixed with 1% formaldehyde, washed, and lysed in ChIP buffer containing protease inhibiters by sonication for 3 s five times with interval of 30 s using ultrasonic disruptor (UR-21P, TOMY) on ice. The debris was removed by centrifugation at 15,000 rpm for 10 min. Lysates were incubated with anti-Ikaros Ab- or rabbit IgG isotype control Ab-coupled Dynabeads M-280 sheep anti-rabbit IgG (VERITAS) with rotation at 4°C overnight. Dynabeads were washed with ChIP buffer, wash buffer, and TE buffer twice each, and DNA was eluted with elution buffer. The eluate was decross-linked by addition of 0.4 mg/ml ProK at 65°C for 2 h and purified by phenol/chloroform and precipitated by 70% ethanol. Quantitative real-time PCR was conducted by THUNDERBIRD SYBR qPCR mix (TOYOBO) using QuantStudio 5 (Thermo Fisher Scientific). Primer pairs used to detect the binding to the *Zbtb16* promoter are as follows: F: 5′-CTCCTGTGGTCAGGCATCAG-3′, R: 5′-CTCAGGATTCGGATCGCATC-3′.

Transfection and reporter assay

The intact proximal promoter of mouse *Zbtb16* (–1,284 to –1) or truncated form (Δ –913 to –732, Δ –0.9 kb) was cloned into the firefly luciferase plasmid vectors (pGL4.10; Promega). Genomic location is based on the sequence of *Zbtb16* (NCBI accession no. NM_001033324.3) mapped on the genomic sequence (NCBI accession no. NC_000075.6 Chromosome 9 Reference GRCm38.p6 C57BL/6) obtained from National Center for Biotechnology Information. Mouse Ikaros, Egr2, and Nfatc2 cDNAs were cloned into the pMX-IRES-GFP vectors. These plasmids were transfected along with a *Renilla* luciferase plasmid vector (pGL4.74; Promega) into HEK293T cells using Polyethylenimine (PEI) MAX

(Polysciences). The luciferase activity was measured using the Dual-Luciferase Reporter Assay System (Promega). Firefly luciferase activity was normalized by *Renilla* luciferase activity.

Identification of Ikaros-binding proteins using BioID

Ikaros cDNA fused to TurboID was cloned into a retroviral vector and transfected into Phoenix retroviral packaging cells using PEI MAX (Polysciences). Culture supernatant containing retroviruses was used for infection into DN32.D3 cells. Cells were cultured in 10% FBS/DMEM, which does not contain biotin for >3 days, and treated with 10 µg/ml of anti-CD3 Ab. After washing cells, 100 µg/ml of goat anti-hamster IgG was added to stimulate cells by TCR cross-linking in the presence of 50 µM D-biotin (Nacalai Tesque) and incubated at 37°C for 45 min. The cells were washed with ice-cold HEPES saline and lysed in Guanidine-TCEP buffer (8 M guanidine-HCl, 100 mM HEPES-NaOH, pH 7.5, 10 mM TCEP, and 40 mM chloroacetamide). The lysates were dissolved by heating and sonication and then centrifuged at 20,000 × *g* for 15 min at 4°C. The supernatants were recovered, and proteins were purified by methanol–chloroform precipitation and solubilized using PTS buffer (12 mM SDC, 12 mM SLS, and 100 mM Tris-HCl, pH 8.0). After sonication and heating, the protein solution was diluted fivefold with 100 mM Tris-HCl, pH 8.0, and digested with trypsin (MS grade, Thermo Fisher Scientific) at 37°C overnight. The resulting peptide solutions were diluted twofold with TBS (50 mM Tris-HCl, pH 7.5, and 150 mM NaCl). Biotinylated peptides were captured on a 15 µl slurry of MagCapture HP Tamavidin 2-REV magnetic beads (FUJIFILM Wako) by incubation for 3 h at 4°C. After washing with TBS five times, the biotinylated peptides were eluted with 100 µl of 1 mM biotin in TBS for 15 min at 37°C twice. The combined eluates were desalted using GL-Tip SDB (GL Sciences), evaporated in a SpeedVac concentrator, and redissolved in 0.1% TFA and 3% ACN.

LC-MS/MS analysis of the resultant peptides was performed on an EASY-nLC 1200 UHPLC connected to an Orbitrap Fusion mass spectrometer through a nanoelectrospray ion source (Thermo Fisher Scientific). The peptides were separated on a C18 reversed-phase column (75 µm × 150 mm; Nikkyo Technos) with a linear 4–32% ACN gradient for 0–60 min, followed by an increase to 80% ACN for 10 min, and a final hold at 80% ACN for 10 min. The mass spectrometer was operated in data-dependent acquisition mode with a maximum duty cycle of 3 s. The MS1 spectra were measured with a resolution of 120,000, an AGC target of 4e5, and a mass range of 375–1,500 *m/z*. HCD MS/MS spectra were acquired in a linear ion trap with an AGC target of 1e4, an isolation window of 1.6 *m/z*, a maximum injection time of 200 ms, and a normalized collision energy of 30. Dynamic exclusion was set to 10 s. Raw data were directly analyzed against the Swiss-Prot database restricted to *M. musculus* using Proteome Discoverer 2.5 (Thermo Fisher Scientific) with the Mascot search engine. The search parameters were as follows: (1) trypsin as an enzyme with up to two missed cleavages, (2) precursor mass tolerance of 10 ppm, (3) fragment mass tolerance of 0.6 Da, (4) carbamidomethylation of cysteine as a fixed modification, and (5) acetylation of protein N terminus, oxidation of methionine, and biotinylation of lysine as variable modifications. Peptides were filtered at an FDR of 1% using the percolator node. Label-free quantification was performed based on the intensities of the precursor ions using the precursor ions quantifier node. Normalization was performed such that the total sum of the abundance values for each sample over all peptides was the same.

TCR reconstitution and stimulation of reporter cells

As TCRβ sequences of some TCR clonotypes with large clone size were not readout in scRNA/TCR-seq analysis, TCR sequences of thymic iNKT cells were analyzed by bulk sequencing using SMARTer mouse TCRα/β profiling kit (Takara). Most detected TCRα and top five TCRβ cDNAs were cloned into retroviral vectors. TCR-lacking mouse T cell hybridoma cells transduced with mouse CD1d were infected with culture supernatant containing retroviruses to reconstitute TCRαβ. Surface expression of introduced TCR was confirmed by staining with anti-CD3 Ab. For stimulation of cells, α-GalCer was suspended in PBS containing 0.5% Tween-20, followed by sonication for 15 min, diluted in 10% FBS/RPMI, and added into cultured cells.

Statistical analysis

All values with error bars are presented as the mean ± SD of multiple samples or assays. Unpaired or paired two-tailed Student's *t* tests or one-way ANOVA followed by Tukey's multiple comparison test were performed for the statistical analysis using Prism 9 software (GraphPad Software). P values <0.05 were considered statistically significant.

Online supplemental material

Fig. S1 shows the T cell population in the thymus of *Cd4*-Cre–mediated T cell–specific PKD-deficient mice. Fig. S2 shows the reactivity of frequent thymic iNKT clonotypes to α-GalCer. Fig. S3 shows the thymic iNKT cell subsets and single cell–based transcriptomes and chromatin accessibility of thymic iNKT cells in PKD-deficient mice. Fig. S4 shows the cell populations in the thymus of *Zbtb16* Tg mice. Fig. S5 shows the generation and characterization of mutant mice.

Data availability

All reagents made for this study are available from the corresponding author upon reasonable request under a standard material transfer agreement. High-throughput sequence data have been deposited to Gene Expression Omnibus database under accession no. GSE288015 (scRNA/TCR-seq and scATAC-seq), GSE288329 (ChIP-seq), and GSE287699 (bulk TCR-seq), respectively. The mass spectrometry proteomics data have been deposited to the ProteomeXchange Consortium via the jPOST partner repository with the dataset identifiers PXD059288 (Fig. 4 B) and PXD059289 (Fig. 5 E).

Acknowledgments

We thank Y. Takeuchi, T. Yoneda, A. Murakami, Y. Erikawa, and E. Ito for technical assistance; C. Schutt for discussion; I. Taniuchi for Tg vector and discussion; K. Nishino and M. Kawano for MS analyses; D. Okuzaki and YC. Liu for bioinformatics data

analysis; M. Taniguchi for providing *Traj18*$^{-/-}$ mice; M. Ikawa, C. Emori, M. Tanaka, Y. Baba, and M. Matsuda for generation of mice; and NIH Tetramer Core Facility (NIH Contract 75N93020D00005 and RRID:SCR_026557) for providing PBS-57–loaded mouse CD1d and 5-OP-RU–loaded mouse MR1 tetramers.

This research was supported by Grant-in-Aid for Scientific Research KAKENHI (JP19K07624 and JP22K07117 [to Eri Ishikawa], JP23H00403, and JP22H05183 [to Sho Yamasaki]) from Japan Society for the Promotion of Science and AMED (JP24wm0325054, JP253fa727001, JP23jk0210005, and JP223fa627002). This work was partly performed in the Joint Usage and Joint Research Programs of the Institute of Advanced Medical Sciences, Tokushima University and the Cooperative Research Project Program of the Medical Institute of Bioregulation, Kyushu University.

Author contributions: Eri Ishikawa: conceptualization, data curation, formal analysis, funding acquisition, investigation, methodology, project administration, resources, validation, visualization, and writing—original draft, review, and editing. Hidetaka Kosako: data curation, investigation, methodology, and writing—review and editing. Daisuke Motooka: data curation, formal analysis, investigation, methodology, resources, software, and writing—review and editing. Mai Imasaka: resources. Hiroshi Watarai: resources. Masaki Ohmuraya: resources. Sho Yamasaki: conceptualization, supervision, and writing—original draft.

Disclosures: The authors declare no competing interests exist.

Submitted: 12 March 2025
Revised: 12 July 2025
Accepted: 18 August 2025

References

Avitahl, N., S. Winandy, C. Friedrich, B. Jones, Y. Ge, and K. Georgopoulos. 1999. Ikaros sets thresholds for T cell activation and regulates chromosome propagation. *Immunity*. 10:333–343. https://doi.org/10.1016/s1074-7613(00)80033-3

Azzam, H.S., A. Grinberg, K. Lui, H. Shen, E.W. Shores, and P.E. Love. 1998. CD5 expression is developmentally regulated by T cell receptor (TCR) signals and TCR avidity. *J. Exp. Med.* 188:2301–2311. https://doi.org/10.1084/jem.188.12.2301

Bendelac, A. 1995. Positive selection of mouse NK1$^+$ T cells by CD1-expressing cortical thymocytes. *J. Exp. Med.* 182:2091–2096. https://doi.org/10.1084/jem.182.6.2091

Bendelac, A., O. Lantz, M.E. Quimby, J.W. Yewdell, J.R. Bennink, and R.R. Brutkiewicz. 1995. CD1 recognition by mouse NK1+ T lymphocytes. *Science*. 268:863–865. https://doi.org/10.1126/science.7538697

Bernardi, C., G. Maurer, T. Ye, P. Marchal, B. Jost, M. Wissler, U. Maurer, P. Kastner, S. Chan, and C. Charvet. 2021. CD4$^+$ T cells require Ikaros to inhibit their differentiation toward a pathogenic cell fate. *Proc. Natl. Acad. Sci. USA*. 118:e2023172118. https://doi.org/10.1073/pnas.2023172118

Birkholz, A.M., and M. Kronenberg. 2015. Antigen specificity of invariant natural killer T-cells. *Biomed. J.* 38:470–483. https://doi.org/10.1016/j.bj.2016.01.003

Boast, B., C.d. J. Nunes-Santos, H.S. Kuehn, and S.D. Rosenzweig. 2021. Ikaros-associated diseases: From mice to humans and back again. *Front. Pediatr.* 9:705497. https://doi.org/10.3389/fped.2021.705497

Bortoluzzi, S., N. Dashtsoodol, T. Engleitner, C. Drees, S. Helmrath, J. Mir, A. Toska, M. Flossdorf, R. Öllinger, M. Solovey, et al. 2021. Brief homogeneous TCR signals instruct common iNKT progenitors whose effector diversification is characterized by subsequent cytokine signaling. *Immunity*. 54:2497–2513.e9. https://doi.org/10.1016/j.immuni.2021.09.003

Brennan, P.J., M. Brigl, and M.B. Brenner. 2013. Invariant natural killer T cells: An innate activation scheme linked to diverse effector functions. *Nat. Rev. Immunol.* 13:101–117. https://doi.org/10.1038/nri3369

Chen, S., C. Cai, Z. Li, G. Liu, Y. Wang, M. Blonska, D. Li, J. Du, X. Lin, M. Yang, and Z. Dong. 2017. Dissection of SAP-dependent and SAP-independent SLAM family signaling in NKT cell development and humoral immunity. *J. Exp. Med.* 214:475–489. https://doi.org/10.1084/jem.20161312

Constantinides, M.G., and A. Bendelac. 2013. Transcriptional regulation of the NKT cell lineage. *Curr. Opin. Immunol.* 25:161–167. https://doi.org/10.1016/j.coi.2013.01.003

Cui, J., T. Shin, T. Kawano, H. Sato, E. Kondo, I. Toura, Y. Kaneko, H. Koseki, M. Kanno, and M. Taniguchi. 1997. Requirement for Valpha14 NKT cells in IL-12-mediated rejection of tumors. *Science*. 278:1623–1626. https://doi.org/10.1126/science.278.5343.1623

Das, R., D.B. Sant'Angelo, and K.E. Nichols. 2010. Transcriptional control of invariant NKT cell development. *Immunol. Rev.* 238:195–215. https://doi.org/10.1111/j.1600-065X.2010.00962.x

Dose, M., B.P. Sleckman, J. Han, A.L. Bredemeyer, A. Bendelac, and F. Gounari. 2009. Intrathymic proliferation wave essential for Valpha14$^+$ natural killer T cell development depends on c-Myc. *Proc. Natl. Acad. Sci. USA*. 106:8641–8646. https://doi.org/10.1073/pnas.0812255106

Dutta, M., Z.J. Kraus, J. Gomez-Rodriguez, S.-H. Hwang, J.L. Cannons, J. Cheng, S.-Y. Lee, D.L. Wiest, E.K. Wakeland, and P.L. Schwartzberg. 2013. A role for Ly108 in the induction of promyelocytic zinc finger transcription factor in developing thymocytes. *J. Immunol.* 190:2121–2128. https://doi.org/10.4049/jimmunol.1202145

Egawa, T., and D.R. Littman. 2008. ThPOK acts late in specification of the helper T cell lineage and suppresses Runx-mediated commitment to the cytotoxic T cell lineage. *Nat. Immunol.* 9:1131–1139. https://doi.org/10.1038/ni.1652

Enders, A., S. Stankovic, C. Teh, A.P. Uldrich, M. Yabas, T. Juelich, J.A. Altin, S. Frankenreiter, H. Bergmann, C.M. Roots, et al. 2012. ZBTB7B (Th-POK) regulates the development of IL-17-producing CD1d-restricted mouse NKT cells. *J. Immunol.* 189:5240–5249. https://doi.org/10.4049/jimmunol.1201486

Engel, I., K. Hammond, B.A. Sullivan, X. He, I. Taniuchi, D. Kappes, and M. Kronenberg. 2010. Co-receptor choice by V alpha14i NKT cells is driven by Th-POK expression rather than avoidance of CD8-mediated negative selection. *J. Exp. Med.* 207:1015–1029. https://doi.org/10.1084/jem.20090557

Engel, I., M. Zhao, D. Kappes, I. Taniuchi, and M. Kronenberg. 2012. The transcription factor Th-POK negatively regulates Th17 differentiation in Vα14i NKT cells. *Blood*. 120:4524–4532. https://doi.org/10.1182/blood-2012-01-406280

Gabriel, C.H., F. Gross, M. Karl, H. Stephanowitz, A.F. Hennig, M. Weber, S. Gryzik, I. Bachmann, K. Hecklau, J. Wienands, et al. 2016. Identification of novel nuclear factor of activated T cell (NFAT)-associated proteins in T cells. *J. Biol. Chem.* 291:24172–24187. https://doi.org/10.1074/jbc.M116.739326

Gioulbasani, M., A. Galaras, S. Grammenoudi, P. Moulos, A.L. Dent, M. Sigvardsson, P. Hatzis, B.L. Kee, and M. Verykokakis. 2020. The transcription factor BCL-6 controls early development of innate-like T cells. *Nat. Immunol.* 21:1058–1069. https://doi.org/10.1038/s41590-020-0737-y

Gleimer, M., H. von Boehmer, and T. Kreslavsky. 2012. PLZF controls the expression of a limited number of genes essential for NKT cell function. *Front. Immunol.* 3:374. https://doi.org/10.3389/fimmu.2012.00374

Godfrey, D.I., and S.P. Berzins. 2007. Control points in NKT-cell development. *Nat. Rev. Immunol.* 7:505–518. https://doi.org/10.1038/nri2116

Godfrey, D.I., S. Stankovic, and A.G. Baxter. 2010. Raising the NKT cell family. *Nat. Immunol.* 11:197–206. https://doi.org/10.1038/ni.1841

Harker, N., T. Naito, M. Cortes, A. Hostert, S. Hirschberg, M. Tolaini, K. Roderick, K. Georgopoulos, and D. Kioussis. 2002. The CD8alpha gene locus is regulated by the Ikaros family of proteins. *Mol. Cell.* 10:1403–1415. https://doi.org/10.1016/s1097-2765(02)00711-6

Hosono, Y., N. Tomiyasu, H. Kasai, E. Ishikawa, M. Takahashi, A. Imamura, H. Ishida, F. Compostella, H. Kida, A. Kumanogoh, et al. 2025. Identification of α-galactosylceramide as an endogenous mammalian antigen for iNKT cells. *J. Exp. Med.* 222:e20240728. https://doi.org/10.1084/jem.20240728

Irie, A., K. Harada, H. Tsukamoto, J.-R. Kim, N. Araki, and Y. Nishimura. 2006. Protein kinase D2 contributes to either IL-2 promoter regulation

or induction of cell death upon TCR stimulation depending on its activity in Jurkat cells. *Int. Immunol.* 18:1737–1747. https://doi.org/10.1093/intimm/dxl108

Ishikawa, E., H. Kosako, T. Yasuda, M. Ohmuraya, K. Araki, T. Kurosaki, T. Saito, and S. Yamasaki. 2016. Protein kinase D regulates positive selection of CD4⁺ thymocytes through phosphorylation of SHP-1. *Nat. Commun.* 7:12756. https://doi.org/10.1038/ncomms12756

Karnaukhov, V.K., A.-L. Le Gac, L. Bilonda Mutala, A. Darbois, L. Perrin, F. Legoux, A.M. Walczak, T. Mora, and O. Lantz. 2024. Innate-like T cell subset commitment in the murine thymus is independent of TCR characteristics and occurs during proliferation. *Proc. Natl. Acad. Sci. USA.* 121:e2311348121. https://doi.org/10.1073/pnas.2311348121

Kastner, P., and S. Chan. 2024. IKAROS family transcription factors in lymphocyte differentiation and function. *Adv. Exp. Med. Biol.* 1459:33–52. https://doi.org/10.1007/978-3-031-62731-6_2

Koay, H.F., N.A. Gherardin, A. Enders, L. Loh, L.K. Mackay, C.F. Almeida, B.E. Russ, C.A. Nold-Petry, M.F. Nold, S. Bedoui, et al. 2016. A three-stage intrathymic development pathway for the mucosal-associated invariant T cell lineage. *Nat. Immunol.* 17:1300–1311. https://doi.org/10.1038/ni.3565

Kondo, M., K. Akashi, J. Domen, K. Sugamura, and I.L. Weissman. 1997. Bcl-2 rescues T lymphopoiesis, but not B or NK cell development, in common gamma chain-deficient mice. *Immunity*. 7:155–162. https://doi.org/10.1016/s1074-7613(00)80518-x

Koshiba, T., and H. Kosako. 2020. Mass spectrometry-based methods for analysing the mitochondrial interactome in mammalian cells. *J. Biochem.* 167:225–231. https://doi.org/10.1093/jb/mvz090

Kovalovsky, D., O.U. Uche, S. Eladad, R.M. Hobbs, W. Yi, E. Alonzo, K. Chua, M. Eidson, H.-J. Kim, J.S. Im, et al. 2008. The BTB-zinc finger transcriptional regulator PLZF controls the development of invariant natural killer T cell effector functions. *Nat. Immunol.* 9:1055–1064. https://doi.org/10.1038/ni.1641

Kovalovsky, D., E.S. Alonzo, O.U. Uche, M. Eidson, K.E. Nichols, and D.B. Sant'Angelo. 2010. PLZF induces the spontaneous acquisition of memory/effector functions in T cells independently of NKT cell-related signals. *J. Immunol.* 184:6746–6755. https://doi.org/10.4049/jimmunol.1000776

Kreslavsky, T., A.K. Savage, R. Hobbs, F. Gounari, R. Bronson, P. Pereira, P.P. Pandolfi, A. Bendelac, and H. von Boehmer. 2009. TCR-inducible PLZF transcription factor required for innate phenotype of a subset of gammadelta T cells with restricted TCR diversity. *Proc. Natl. Acad. Sci. USA.* 106:12453–12458. https://doi.org/10.1073/pnas.0903895106

Lantz, O., and A. Bendelac. 1994. An invariant T cell receptor alpha chain is used by a unique subset of major histocompatibility complex class I-specific CD4⁺ and CD4⁻8⁻ T cells in mice and humans. *J. Exp. Med.* 180:1097–1106. https://doi.org/10.1084/jem.180.3.1097

Lee, P.P., D.R. Fitzpatrick, C. Beard, H.K. Jessup, S. Lehar, K.W. Makar, M. Pérez-Melgosa, M.T. Sweetser, M.S. Schlissel, S. Nguyen, et al. 2001. A critical role for Dnmt1 and DNA methylation in T cell development, function, and survival. *Immunity*. 15:763–774. https://doi.org/10.1016/s1074-7613(01)00227-8

Lee, Y.J., K.L. Holzapfel, J. Zhu, S.C. Jameson, and K.A. Hogquist. 2013. Steady-state production of IL-4 modulates immunity in mouse strains and is determined by lineage diversity of iNKT cells. *Nat. Immunol.* 14:1146–1154. https://doi.org/10.1038/ni.2731

Liu, X., S. Yin, W. Cao, W. Fan, L. Yu, L. Yin, L. Wang, and J. Wang. 2014. Runt-related transcription factor 3 is involved in the altered phenotype and function in ThPok-deficient invariant natural killer T cells. *Cell. Mol. Immunol.* 11:232–244. https://doi.org/10.1038/cmi.2014.3

Malissen, M., A. Gillet, L. Ardouin, G. Bouvier, J. Trucy, P. Ferrier, E. Vivier, and B. Malissen. 1995. Altered T cell development in mice with a targeted mutation of the CD3-epsilon gene. *EMBO J.* 14:4641–4653. https://doi.org/10.1002/j.1460-2075.1995.tb00146.x

Mao, A.P., M.G. Constantinides, R. Mathew, Z. Zuo, X. Chen, M.T. Weirauch, and A. Bendelac. 2016. Multiple layers of transcriptional regulation by PLZF in NKT-cell development. *Proc. Natl. Acad. Sci. USA.* 113:7602–7607. https://doi.org/10.1073/pnas.1601504113

Mao, A.-P., I.E. Ishizuka, D.N. Kasal, M. Mandal, and A. Bendelac. 2017. A shared Runx1-bound Zbtb16 enhancer directs innate and innate-like lymphoid lineage development. *Nat. Commun.* 8:863. https://doi.org/10.1038/s41467-017-00882-0

Matsumoto, Y., K. Kishida, M. Matsumoto, S. Matsuoka, M. Kohyama, T. Suenaga, and H. Arase. 2021. A TCR-like antibody against a proinsulin-containing fusion peptide ameliorates type 1 diabetes in NOD mice. *Biochem. Biophys. Res. Commun.* 534:680–686. https://doi.org/10.1016/j.bbrc.2020.11.019

Matthews, S.A., M.N. Navarro, L.V. Sinclair, E. Emslie, C. Feijoo-Carnero, and D.A. Cantrell. 2010. Unique functions for protein kinase D1 and protein kinase D2 in mammalian cells. *Biochem. J.* 432:153–163. https://doi.org/10.1042/BJ20101188

Muroi, S., Y. Naoe, C. Miyamoto, K. Akiyama, T. Ikawa, K. Masuda, H. Kawamoto, and I. Taniuchi. 2008. Cascading suppression of transcriptional silencers by ThPOK seals helper T cell fate. *Nat. Immunol.* 9:1113–1121. https://doi.org/10.1038/ni.1650

Ren, Y., N. Dashtsoodol, H. Watarai, H. Koseki, C. Quan, and M. Taniguchi. 2014. Generation of induced pluripotent stem cell-derived mice by reprogramming of a mature NKT cell. *Int. Immunol.* 26:551–561. https://doi.org/10.1093/intimm/dxu057

Rey, O., J. Sinnett-Smith, E. Zhukova, and E. Rozengurt. 2001. Regulated nucleocytoplasmic transport of protein kinase D in response to G protein-coupled receptor activation. *J. Biol. Chem.* 276:49228–49235. https://doi.org/10.1074/jbc.M109395200

Rozengurt, E., O. Rey, and R.T. Waldron. 2005. Protein kinase D signaling. *J. Biol. Chem.* 280:13205–13208. https://doi.org/10.1074/jbc.R500002200

Savage, A.K., M.G. Constantinides, J. Han, D. Picard, E. Martin, B. Li, O. Lantz, and A. Bendelac. 2008. The transcription factor PLZF directs the effector program of the NKT cell lineage. *Immunity*. 29:391–403. https://doi.org/10.1016/j.immuni.2008.07.011

Seiler, M.P., R. Mathew, M.K. Liszewski, C.J. Spooner, K. Barr, F. Meng, H. Singh, and A. Bendelac. 2012. Elevated and sustained expression of the transcription factors Egr1 and Egr2 controls NKT lineage differentiation in response to TCR signaling. *Nat. Immunol.* 13:264–271. https://doi.org/10.1038/ni.2230

Takeuchi, Y., K. Hirota, and S. Sakaguchi. 2020. Impaired T cell receptor signaling and development of T cell-mediated autoimmune arthritis. *Immunol. Rev.* 294:164–176. https://doi.org/10.1111/imr.12841

Taniuchi, I., M. Osato, T. Egawa, M.J. Sunshine, S.C. Bae, T. Komori, Y. Ito, and D.R. Littman. 2002. Differential requirements for Runx proteins in CD4 repression and epigenetic silencing during T lymphocyte development. *Cell*. 111:621–633. https://doi.org/10.1016/s0092-8674(02)01111-x

Tuttle, K.D., S.H. Krovi, J. Zhang, R. Bedel, L. Harmacek, L.K. Peterson, L.L. Dragone, A. Lefferts, C. Halluszczak, K. Riemondy, et al. 2018. TCR signal strength controls thymic differentiation of iNKT cell subsets. *Nat. Commun.* 9:2650. https://doi.org/10.1038/s41467-018-05026-6

Uckun, F.M., H. Ma, J. Zhang, Z. Ozer, S. Dovat, C. Mao, R. Ishkhanian, P. Goodman, and S. Qazi. 2012. Serine phosphorylation by SYK is critical for nuclear localization and transcription factor function of Ikaros. *Proc. Natl. Acad. Sci. USA.* 109:18072–18077. https://doi.org/10.1073/pnas.1209828109

Wang, H., and K.A. Hogquist. 2018. How lipid-specific T cells become effectors: The differentiation of iNKT subsets. *Front. Immunol.* 9:1450. https://doi.org/10.3389/fimmu.2018.01450

Wang, L., K.F. Wildt, E. Castro, Y. Xiong, L. Feigenbaum, L. Tessarollo, and R. Bosselut. 2008a. The zinc finger transcription factor Zbtb7b represses CD8-lineage gene expression in peripheral CD4⁺ T cells. *Immunity*. 29:876–887. https://doi.org/10.1016/j.immuni.2008.09.019

Wang, L., K.F. Wildt, J. Zhu, X. Zhang, L. Feigenbaum, L. Tessarollo, W.E. Paul, B.J. Fowlkes, and R. Bosselut. 2008b. Distinct functions for the transcription factors GATA-3 and ThPOK during intrathymic differentiation of CD4⁺ T cells. *Nat. Immunol.* 9:1122–1130. https://doi.org/10.1038/ni.1647

Watarai, H., S.-i. Fujii, D. Yamada, A. Rybouchkin, S. Sakata, Y. Nagata, M. Iida-Kobayashi, E. Sekine-Kondo, K. Shimizu, Y. Shozaki, et al. 2010. Murine induced pluripotent stem cells can be derived from and differentiate into natural killer T cells. *J. Clin. Invest.* 120:2610–2618. https://doi.org/10.1172/JCI42027

Winandy, S., L. Wu, J.H. Wang, and K. Georgopoulos. 1999. Pre-T cell receptor (TCR) and TCR-controlled checkpoints in T cell differentiation are set by Ikaros. *J. Exp. Med.* 190:1039–1048. https://doi.org/10.1084/jem.190.8.1039

Zhao, M., M.N.D. Svensson, K. Venken, A. Chawla, S. Liang, I. Engel, P. Mydel, J. Day, D. Elewaut, N. Bottini, and M. Kronenberg. 2018. Altered thymic differentiation and modulation of arthritis by invariant NKT cells expressing mutant ZAP70. *Nat. Commun.* 9:2627. https://doi.org/10.1038/s41467-018-05095-7

Supplemental material

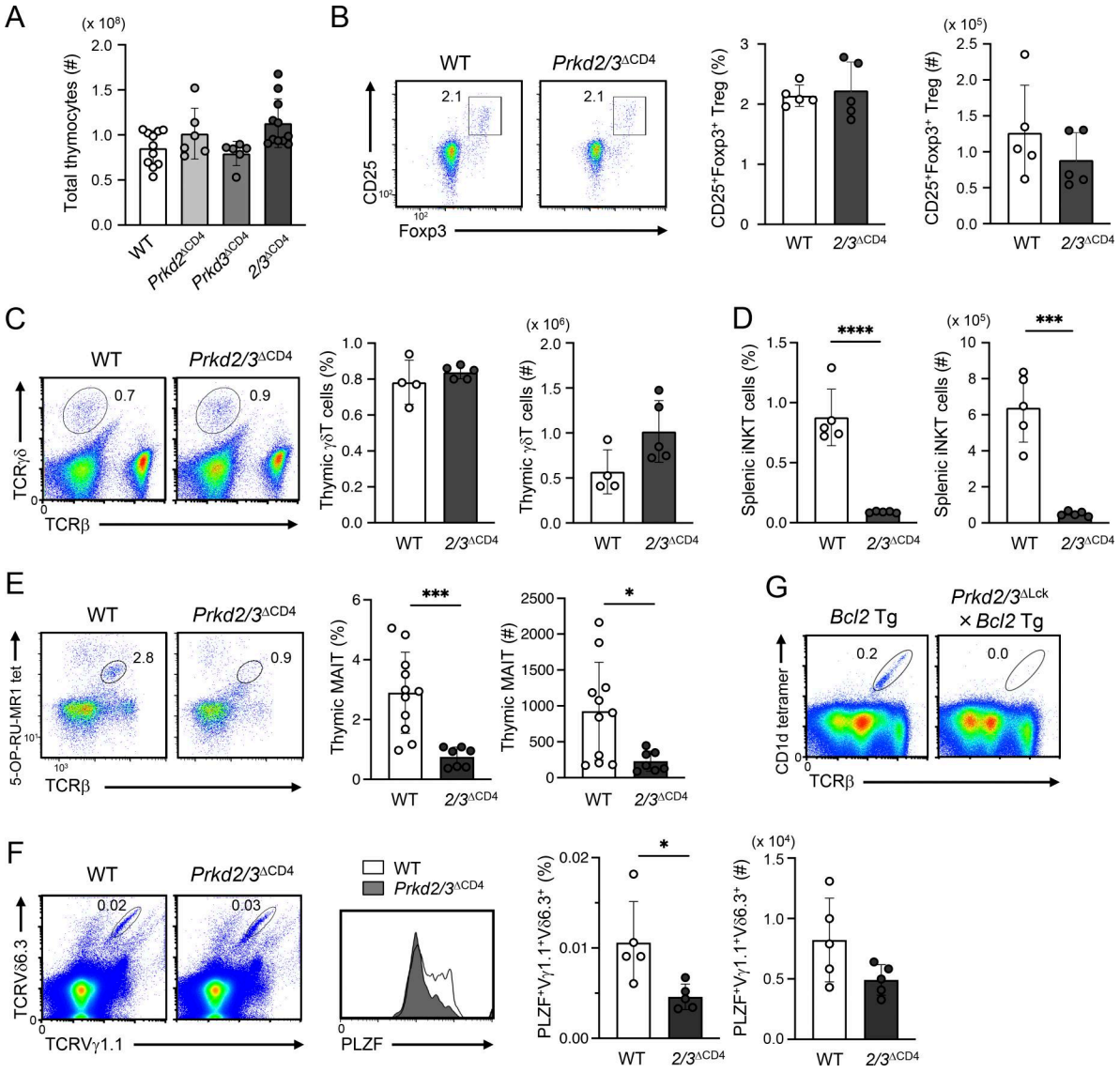

Figure S1. **Development of various T cell subsets in *Prkd2/3*$^{\Delta CD4}$ mice. (A)** Total thymocyte numbers in indicated mouse strains. Each symbol represents an individual mouse (n = 6–11), and the bar graphs indicate mean ± SD of cell numbers. **(B)** Representative FACS profiles of CD25 and Foxp3 expression (left) and bar graphs of the proportions (middle) and cell numbers (right) of CD25⁺Foxp3⁺ Treg cells in WT and *Prkd2/3*$^{\Delta CD4}$ thymus (n = 5). **(C)** Representative FACS profiles of TCRβ and TCRγδ expression (left) and bar graphs of the proportions (middle) and cell numbers (right) of γδT cells in WT and *Prkd2/3*$^{\Delta CD4}$ thymus (n = 4–5). **(D)** Proportions (left) and cell numbers (right) of iNKT cells in the spleen of WT and *Prkd2/3*$^{\Delta CD4}$ mice (n = 5). **(E)** Representative FACS profiles of MAIT cells (left) and bar graphs of the proportions (middle) and cell numbers (right) of MAIT cells in WT and *Prkd2/3*$^{\Delta CD4}$ thymus (n = 7–11). **(F)** Representative FACS profiles of TCRVγ1.1⁺TCRVδ6.3⁺ cells and the expression of PLZF in TCRVγ1.1⁺ TCRVδ6.3⁺ cells from WT and *Prkd2/3*$^{\Delta CD4}$ thymus (left panels). The proportions and cell numbers of PLZF⁺ TCRVγ1.1⁺TCRVδ6.3⁺ cells are shown in bar graphs (n = 5) (right panels). **(G)** Representative FACS profiles of iNKT cells in the thymus from *Bcl2* Tg and *Prkd2/3*$^{\Delta Lck}$×*Bcl2* Tg mice. Each symbol represents an individual mouse, and the bar graphs indicate mean ± SD of proportions or cell numbers (A–F). Data are representative of two independent experiments (G). Statistical significance was determined by unpaired two-tailed Student's t test (D–F). *P < 0.05, ***P < 0.001, and ****P < 0.0001.

A

	TCRαβ#	TRAV	CDR3α	TRAJ	TRBV	CDR3β	TRBJ
WT	TCRαβ1	11	CVVGDRGSALGRLHF	18	29	CASSFSGTGDSDYTF	1-2
	TCRαβ2	11	CVVGDRGSALGRLHF	18	13-3	CASTHWGGAETLYF	2-3
	TCRαβ3	11	CVVGDRGSALGRLHF	18	13-1	CASSDRGEQYF	2-7
	TCRαβ4	11	CVVGDRGSALGRLHF	18	13-1	CASRSGHNNQAPLF	1-5
Prkd2/3$^{\Delta CD4}$	TCRαβ1	11	CVVGDRGSALGRLHF	18	13-1	CASSEGYEQYF	2-7
	TCRαβ2	11	CVVGDRGSALGRLHF	18	17	CASSRTGGQDTQYF	2-5
	TCRαβ3	11	CVVGDRGSALGRLHF	18	29	CASSLWDNYAEQFF	2-1
	TCRαβ4	11	CVVGDRGSALGRLHF	18	13-2	CASGDGTGEQYF	2-7
	TCRαβ5	11	CVVGDRGSALGRLHF	18	13-1	CASSGTGTGSYEQYF	2-7

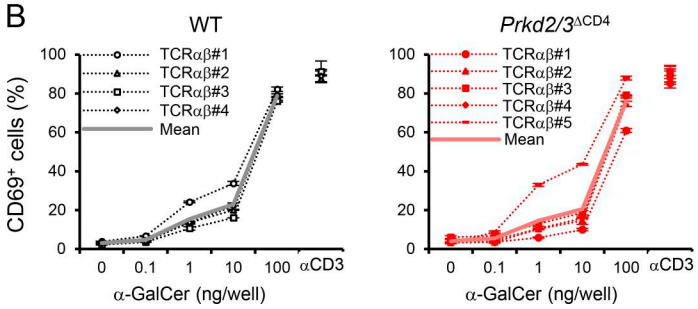

Figure S2. **Reactivity of frequent iNKT cell clonotypes in PKD-deficient mice to α-GalCer. (A)** Most frequent TCRα and the top 5 frequent TCRβs detected in bulk TCR-seq analysis of WT and *Prkd2/3*$^{\Delta CD4}$ thymic iNKT cells. Each paired TCRαβ was reconstituted into a mouse T cell hybridoma lacking TCR expression. One of the TCRs from WT iNKT cells was not detected on the cell surface and, therefore, removed from the data. **(B)** T cell hybridoma cells reconstituted with iNKT TCRαβ listed in A from WT (left) or *Prkd2/3*$^{\Delta CD4}$ (right) and mouse CD1d were stimulated with the indicated amounts of α-GalCer in a 96-well plate. The proportion of cells expressing an activation marker CD69 was analyzed by flow cytometry after 16 h (line graphs, dotted lines). Mean proportion of CD69-expressing cells is overlaid (solid lines). Stimulation with plate-coated anti-CD3 Ab was used as positive control (right symbols). Data are presented as the mean ± SD of triplicate assays and representative of two independent experiments.

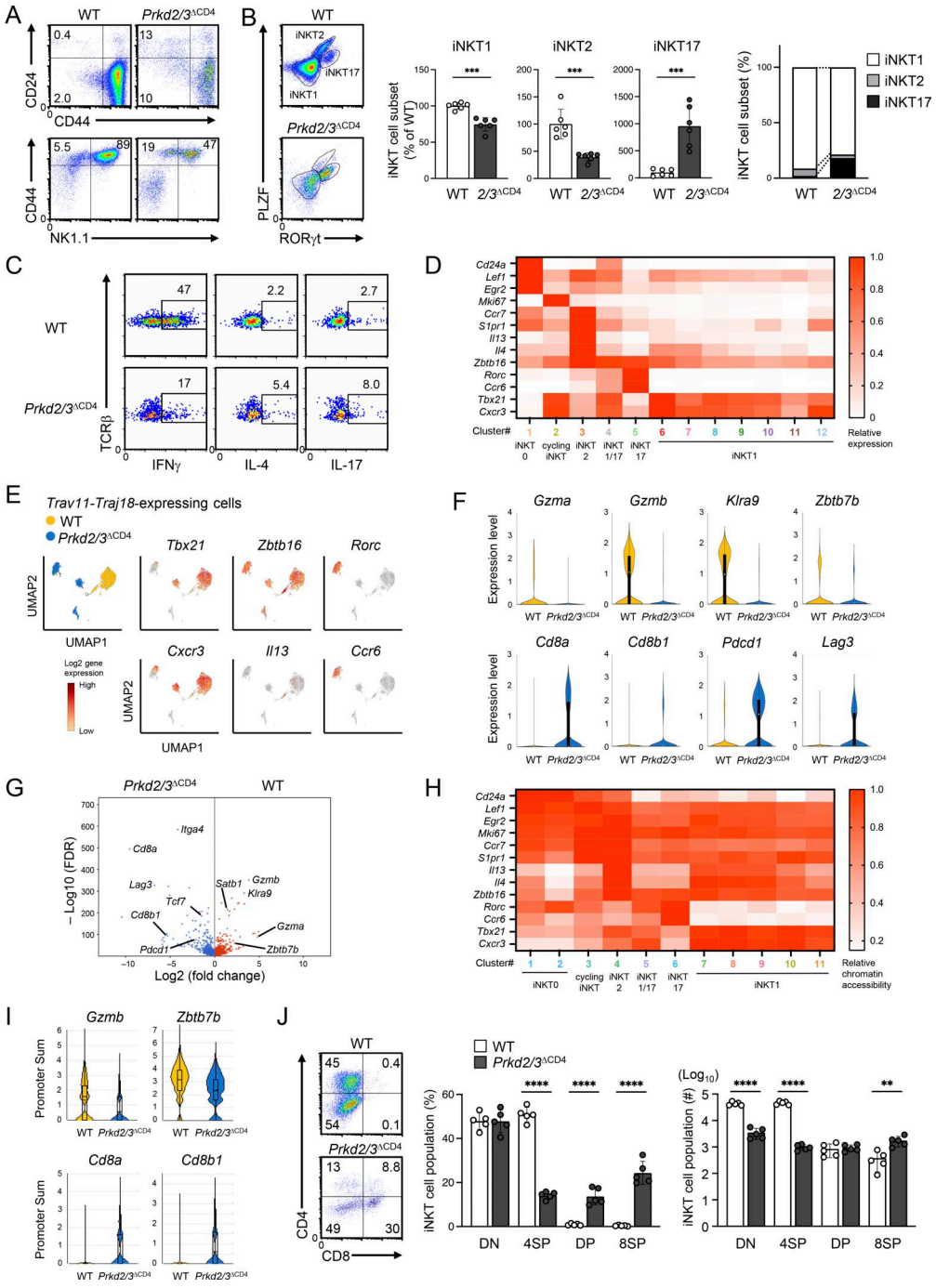

Figure S3. **Defective iNKT cell development in PKD-deficient mice. (A)** Analysis of maturation stages of WT and *Prkd2/3*$^{\Delta CD4}$ thymic iNKT cells. Representative FACS profiles are shown. **(B)** Analysis of WT and *Prkd2/3*$^{\Delta CD4}$ thymic iNKT cell subsets. Representative FACS profiles (left) and bar graphs of the relative proportions to WT mice (middle) and average proportions (right) of CD1d tetramer^{+} iNKT cells at each subset in tetramer-enriched thymocytes. Each symbol represents an individual mouse (n = 6), and the bar graphs indicate mean ± SD of relative proportions (middle). **(C)** Expressions of IFNγ, IL-4, and IL-17 in CD1d tetramer^{+} thymic iNKT cells after stimulation with PMA and ionomycin for 4 h. **(D)** Expression of representative genes in each thymic iNKT cell subset. Relative expressions to the maximum expression are shown as a heatmap. The color of each cluster# matches to that of cells in each cluster in Fig. 2 D. **(E)** *Trav11-Traj18*–expressing cells defined by scTCR-seq analysis were sub-clustered by cell identity. Expressions of selected gene markers of iNKT1 (*Tbx21* and *Cxcr3*), iNKT2 (*Zbtb16* and *Il13*), and iNKT17 (*Rorc* and *Ccr6*) cells are shown as heatmaps in the UMAP plot. **(F)** Differentially expressed genes in WT and *Prkd2/3*$^{\Delta CD4}$ thymic iNKT cells. Expression levels of representative genes are shown as violin plots. **(G)** Volcano plot of differentially expressed genes in WT and *Prkd2/3*$^{\Delta CD4}$ iNKT cells within the iNKT1 cell clusters. **(H)** Chromatin accessibility of representative genes in each thymic iNKT cell subset. Relative chromatin accessibilities to the maximum are shown as a heatmap. The color of each cluster# matches to that of cells in each cluster in Fig. 2 E. **(I)** Differentially enriched accessibilities to the promoter region of each gene, which are defined as promoter sums, in WT and *Prkd2/3*$^{\Delta CD4}$ iNKT cells. Promoter sums of representative genes are shown as violin plots. **(J)** Representative FACS profiles of CD4 and CD8 expression on WT and *Prkd2/3*$^{\Delta CD4}$ thymic iNKT cells (left) and bar graphs of the proportions (middle) and cell numbers (right) of DN, DP, 4SP, and 8SP iNKT cells (n = 5). Data are representative of three independent experiments (A and C). Statistical significance was determined by unpaired two-tailed Student's t test (B and J). **P < 0.01, ***P < 0.001, and ****P < 0.0001.

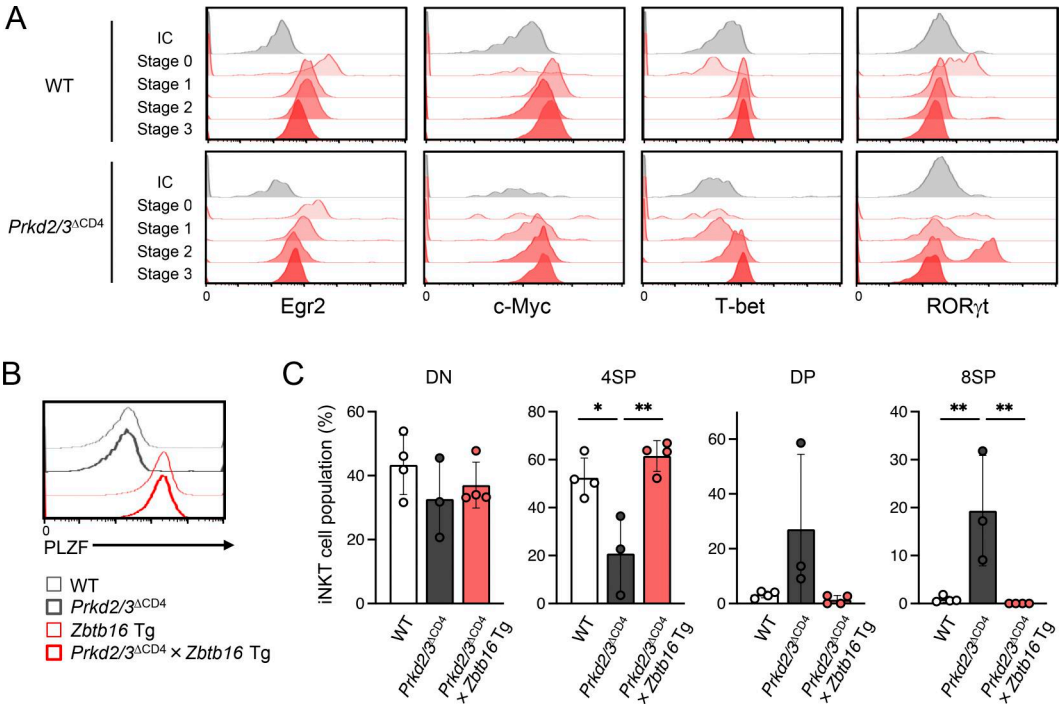

Figure S4. **The expression of transcription factors and iNKT subsets in PKD-deficient mice bearing *Zbtb16* transgene. (A)** Protein expression of Egr2, c-Myc, T-bet, and RORγt in CD1d tetramer⁺ thymic iNKT cells at each maturation stage. IC, iNKT cells stained with isotype control Ab. **(B)** Expression of PLZF in thymocytes from indicated mouse strains. Data are representative of three independent experiments. **(C)** Proportions of DN, 4SP, DP, and 8SP iNKT cells in thymic CD1d tetramer⁺ iNKT cells from WT, *Prkd2/3*$^{\Delta CD4}$, and *Prkd2/3*$^{\Delta CD4}$ × *Zbtb16* Tg mice. Each symbol represents an individual mouse (n = 3–4), and the bar graphs indicate mean ± SD of proportions. Statistical significance was determined by one-way ANOVA followed by Tukey's multiple comparison test. *P < 0.05 and **P < 0.01.

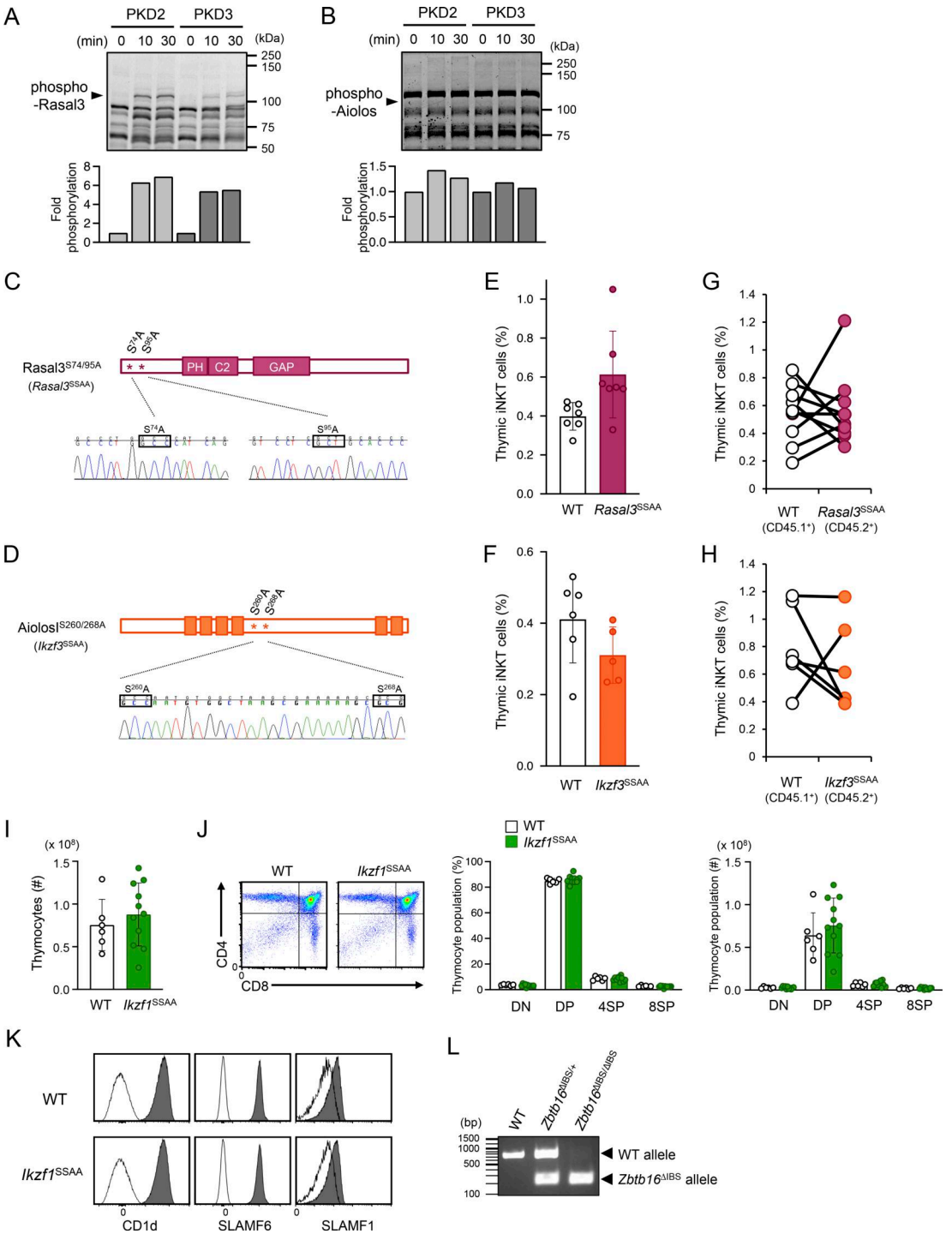

Figure S5. **Generation and characterization of mutant mice lacking phosphorylation sites or Ikaros-binding region. (A and B)** Phos-tag SDS-PAGE of GST-Rasal3 (A) or GST-Aiolos (B) after *in vitro* kinase assay in the presence of recombinant active PKD2 or PKD3 for indicated times. The arrowheads indicate the phosphorylated forms. Phosphorylated bands were quantified and presented as relative to those at 0 min. **(C and D)** Schematic protein structures of phosphorylation-defective mutant Rasal3 (C) or Aiolos (D) and genomic sequence analysis of knock-in alleles. Six orange boxes (D) represent zinc finger domains. **(E and F)** Proportions of CD1d tetramer$^+$ iNKT cells in the thymus from WT and *Rasal3*^{SSAA} (E) or *Ikzf3*^{SSAA} (F) mice. Each symbol represents an individual mouse (n = 7 in E and n = 5–6 in F). The bar graphs indicate mean ± SD of proportions. **(G and H)** iNKT cell generation in the thymus of *Cd3e*$^{\Delta5/\Delta5}$ mice that were transferred with a mixture of Ly5.1$^+$ WT and Ly5.2$^+$ *Rasal3*^{SSAA} (G) or *Ikzf3*^{SSAA} (H) BM cells. Each line graph indicates an individual mouse (n = 9 in G and n = 6 in H). **(I)** Total thymocyte numbers in WT and *Ikzf1*$^{S267/275A}$ (*Ikzf1*^{SSAA}) mice (n = 6–11). **(J)** Representative FACS profiles of CD4 and CD8 expression on thymocytes (left) and bar graphs of the proportions (middle) and cell numbers (right) of DN, DP, 4SP, and 8SP cells from WT and *Ikzf1*^{SSAA} mice (n = 6–11). Each symbol represents an individual mouse, and the bar graphs indicate mean ± SD of proportions or cell numbers. **(K)** Cell surface expression of CD1d, SLAMF6, and SLAMF1 on DP thymocytes from WT and *Ikzf1*^{SSAA} mice. Open histograms, no stain. Filled histograms, Ab stain. **(L)** Genomic PCR of WT, hetero and homo *Zbtb16*$^{\Delta IBS}$ mice. Genomic DNAs were amplified using primers that crossover deleted region. Arrowheads indicate WT and *Zbtb16*$^{\Delta IBS}$ alleles. Data are representative of two (A and B) or three (K and L) independent experiments. Source data are available for this figure: SourceData FS5.